Check for updates

Nanoscale
Advances

rsc.li/nanoscale-advances

Volume 1
Number 1
January 2018
Pages 1-200

ROYAL SOCIETY
OF CHEMISTRY

NCNST

ISSN 2516-0230

ROYAL SOCIETY
OF CHEMISTRY

rsc.li/nanoscale-advances

No primary research results, software or code have been included and no new data were generated or analysed as part of this review.

Facet-controlled growth and soft-chemical exfoliation of two-dimensional titanium dioxide nanosheets

Christian Harito[1], Munawar Khalil[2], Leanddas Nurdiwijayanto[3], Ni Luh Wulan Septiani[4], Syauqi Abdurrahman Abrori[5], Budi Riza Putra[6], Syed Z.J. Zaidi[7], Takaaki Taniguchi[3], Brian Yuliarto[8, 9], Frank C. Walsh[10]

[1] Industrial Engineering Department, BINUS Graduate Program – Master of Industrial Engineering, Bina Nusantara University, Jakarta, Indonesia
[2] Department of Chemistry, Faculty of Mathematics and Natural Sciences, Universitas Indonesia, Kampus Baru UI, Depok, Jawa Barat, Indonesia
[3] Research Center for Materials Nanoarchitectonics (MANA), National Institute for Materials Science (NIMS), 1-1 Namiki, Tsukuba, Ibaraki 305-0044, Japan
[4] Research Center for Advanced Materials, National Research and Innovation Agency, Komplek PUSPIPTEK, Serpong, South Tangerang 15314, Banten, Indonesia
[5] Bina Nusantara University, Jakarta, Indonesia
[6] Research Center for Metallurgy, National Research and Innovation Agency (BRIN), PUSPIPTEK Area, Building No. 470, Setu Regency, South Tangerang, Banten 15314, Indonesia
[7] Institute of Chemical Engineering and Technology, University of the Punjab, Lahore, Pakistan
[8] Advanced Functional Materials Laboratory, Department of Engineering Physics, Institute of Technology Bandung (ITB), Bandung, 40132, Indonesia
[9] Research Center for Nanosciences and Nanotechnology (RCNN), Institute of Technology Bandung (ITB), Bandung, 40132, Indonesia
[10] Electrochemical Engineering Laboratory, Faculty of Engineering and Physical Sciences, University of Southampton, Southampton, UK

Abstract

TiO_2 remains as one of the most popular materials used in catalysts, photovoltaics, coatings, and electronics due to its abundance, chemical stability, and excellent catalytic properties. The tailoring of TiO_2 structure into two-dimensional nanosheets prompted the success of isolation of graphene and MXenes. In this review, facet-controlled TiO_2 and monolayer titanate are outlined, covering their synthesis route and formation mechanism. The reactive facet of TiO_2 is usually controlled by capping agent. In contrast, the monolayer titanate is achieved by ion-exchange and delamination of layered titanates. Each route leads to 2D structures with unique physical and chemical properties, which expands its utilisation into several niche applications. We elaborate the detailed outlook for future use of, and research into, facet-controlled TiO_2 and monolayer titanates. The advantages and disadvantages of both structures are provided along with suggested applications for each type of 2D TiO_2 nanosheets.

Keywords: TiO_2, nanosheets, exposed facets, exfoliation, titania.

List of Abbreviations

[bmim]-[BF4]	1-Butyl-3-methylimidazolium tetrafluoroborate
2D	two dimension
3D	three dimension
AFM	atomic force microscopy
APTES	3-aminopropyl triethoxysilane

ASTL	atomic stacking transporting layer
CB	conduction band
CBM	conduction band minimum
CIP	charged ciprofloxacin
DETA	diethylenetriamine
DFT	density functional theory
DMF	N,N-dimethylformamide
DNA	deoxyribonucleic acid
DSSC	dye-sensitized solar cells
EBD	electron beam deposition
EDTA	ethylenediaminetetraacetic acid
ETL	electron-transporting layer
FESEM	field emmission scanning electron microscopy
HF	hydrofluoric acid
IgG	immunoglobulin G
ITO	indium-doped tin oxide
MB	methylene blue
MO	methyl orange
MXenes	two-dimensional transition metal carbide
NTA	nanotube titanic acid
PET	poly(ethylene-terephthalate)
PFC	photocatalytic fuel cell
PVP	poly(vinylpyrrolidone)
rGO	reduced graphene oxide
SAXS	small-angle X-ray scattering
SDS	sodium dodecyl sulfate
SEM	scanning electron microscopy
SSA	specific surface area

TBA	tetrabutylammonium
TEM	tranmission electron microscopy
TiNS	titania nanosheets
TIP	titanium isopropoxide
TMA	tetramethylammonium
TOB	truncated octahedral bipyramidal
UV	ultraviolet
UV-vis	ultraviolet-visible light
VBM	valence band maximum
XRD	X-ray diffraction

1. Introduction

Titanium, as the 9th most abundant element in the Earth's crust, is naturally found in the form of oxide minerals, particularly titania, TiO_2. Over the last fifty years, TiO_2 has been utilised in many applications involving photocatalysts, photovoltaics, corrosion/UV protection coatings, and electronics while further studies exploring novel uses continue. Modification of titanium oxide morphology into tailored nanostructures is sought by many practitioners since it is able to amplify functionality due to a larger active surface area leading to higher reactivity. Many unique properties can only be observed at the nanoscale regime. For instance, quantum confinement may occur at a nanoscale thickness, tuning in the density of states and band gap of nanomaterials [1]. In catalysis, the exposed facets (surface orientation) of nanomaterials play a crucial role. Certain facets may have higher catalytic activity due to their crystallographic orientation, making them more effective in promoting chemical reactions. For titania, quantum confinement and surface orientation play a major role in photoconversion efficiency [2].

Since the rise of graphene over the last two decades [3], the promise of this unique material has accelerated research interest in inorganic 2D nanomaterials. The rapid development of 2D nanomaterials is not limited to carbonaceous materials. Recently, titanium carbide based 2D nanosheets, known as MXenes, have received much attention. Since 2011, an article on the exfoliation of MXenes (i.e., Ti_3AlC_2) by HF has received over 2500 citations [4], indicating the rapid growth of research. Titanium oxide nanosheets, as a 2D analogue of MXenes, have also shown an academic impact, especially in catalysis; A 2008 contribution on anatase TiO_2 with exposed facets has been cited over 3000 times [5]. Titania itself has enjoyed a huge impact, which have helped transform our knowledge of photoelectrochemical cells since 1972 [6]. Titanium oxide based nanosheets is an important research topic which merits a comprehensive review to update our fundamental knowledge and awareness of their uses.

2D nanosheets typically have a thickness of a few nanometre. They can be divided into three categories, namely exposed facet TiO_2 nanosheets, multi-layered nanosheets and monolayered nanosheets. Exposed facet TiO_2 nanosheets are thin non-layered materials with a 3D

crystallographic structure (i.e., TiO_2 with dominant {001} facets) in Figure 1a. The thickness of this type of nanosheets could reach <5 nm while maintaining the crystallographic structure of TiO_2 [7]. Meanwhile, layered titanium oxide nanosheets consist of thin layer structures made from TiO_6 octahedra in Figure 1b. Monolayered or single-layered titanium oxide nanosheets has been extensively researched by Sasaki *et al.* [8] who discover two-step method to exfoliate titanium oxide (titanate) nanosheets in 1998. In contrast to research on exposed facets TiO_2, which mainly focuses on photocatalysis, research on the monolayered titanate nanosheets extends the exploration of their functionalities/properties, such as dielectric characteristics, together with spin-electronic applications [9]. While titanium oxide nanosheets have potential in electrochemistry [10–12], applications remain exploratory.

2D TiO_2 nanosheets also offer distinct advantages over other 2D materials primarily due to their exceptional chemical stability and abundant availability. For example, MXenes, while promising for various applications, often suffer from oxidation and stability issues, limiting their long-term usability in harsh environments. In contrast, TiO_2 nanosheets are highly resistant to chemical degradation, ensuring consistent performance over time. Meanwhile, graphene, though renowned for its exceptional electrical conductivity and mechanical strength, it often lacks the inherent photocatalytic properties of TiO_2 nanosheets. This makes them less suitable for environmental remediation and energy conversion applications, such as photocatalytic water splitting and pollutant degradation. Besides, producing high-quality graphene can be expensive and challenging to scale up, whereas TiO_2 nanosheets are more cost-effective and accessible in large quantities.

Considering their advantages, this review aims to offer a comprehensive perspective on both the synthesis techniques and the distinct material properties of two key types: exposed facet TiO_2 nanosheets and monolayer titanates. Special attention is devoted to their applications, ranging from energy storage solutions such as sodium and potassium ion batteries to environmental remediation efforts including ion-exchange processes. Moreover, we delve into the advantages and challenges of various synthesis routes, particularly emphasizing the trend toward non-fluorine-based precursors as a safer, more sustainable approach. A forward-looking discussion is included, highlighting the potential of these nanomaterials present in diverse scientific and industrial sectors. Future research directions aimed at optimizing these materials for electrochemical applications and potential integrations with other technologies are also considered.
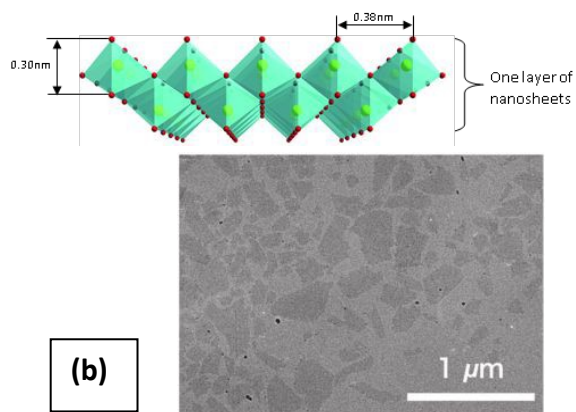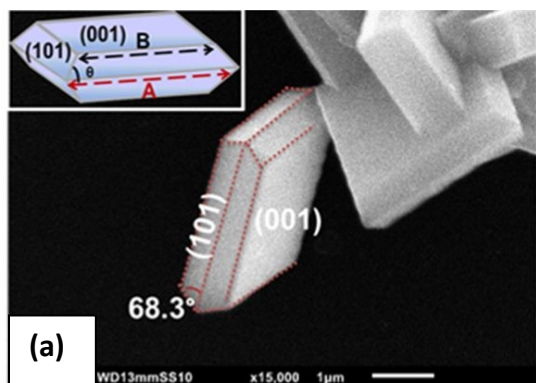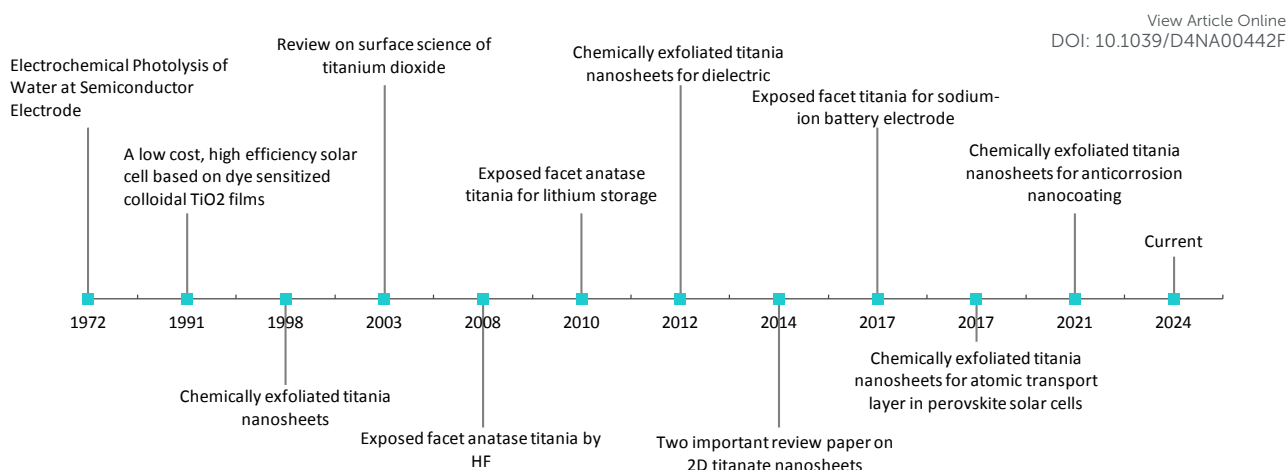
Figure 1. (a) SEM image of exposed {001} facet of TiO_2 with illustration (inset) [13]; (b) TEM image of chemically exfoliated titania nanosheets and its 2D structure [14]; (c) Historical timeline from ground-breaking classic research on TiO_2 [6,15] to the development of exposed facet TiO_2 [5,10–13,16] and single-layered titania nanosheets [8,17–19]. Panel (a) is adapted with permission. [13] Copyright © 2017 American Chemical Society Society. Panel (b) is adapted with permission from John Wiley and Sons. [14] Copyright © 2010 WILEY-VCH.

2. Synthesis routes and mechanism

2.1. Exposed facets titania

Over the last fifty years, crystal facet engineering has been attracting increased attention as one of the most promising ways to enhance both the physical and chemical properties of solid-state materials. Exposing specific types of crystal facets of materials has been reported to be responsible not only for the increased catalytic activity but also specialised optical and electronic properties [20–23]. A similar approach has been applied to TiO_2, considering its great potential in energy and environmental-related applications. Considerable effort has been made to develop a facile and straightforward synthetic protocol for the synthesis of TiO_2 with specific control over particular crystal facets. Using both experimental and theoretical calculations, it is reported that several TiO_2 physicochemical properties, such as catalytic activity, adsorption capability, surface atomic configuration, optoelectronic properties, and catalytic selectivity, could be affected by the type and degree of crystal facet exposure [24–28]. Nevertheless, exposing the desired crystal facet of TiO_2 during its crystal growth is a very challenging task. For instance, under equilibrium condition, most of the available anatase TiO_2 crystals involve by the thermodynamically stable {101} facet due to its low surface free energy (0.44 J m^{-2}) [5,29,30]. High surface free energy facets, such as {001} (0.90 J m^{-2}) and {010} (0.53 J m^{-2}), quickly diminish during crystal growth due to their instability [31].

In general, control synthesis of titania with well-defined crystal facets can be achieved using different routes, i.e., gas oxidation, epitaxial growth, spray-drying, topotactic transformation, crystallization transformation from amorphous TiO_2 and wet-chemical syntheses such as hydrothermal, solvothermal or non-hydrolytic routes [32–37]. However, hydrothermal and solvothermal synthetic routes are mostly preferred for the scalable fabrication of two-dimensional TiO_2 nanostructures. This is primarily due to their ability to offer several beneficial advantages, such as low cost and high ability to direct crystal growth and nucleation by only controlling reaction parameters. Typically, one of the most common strategies for exposing specific types of crystal facets in TiO_2 is by the utilization of an appropriate capping agent during hydrothermal or solvothermal reaction [38–41]. ~~Commonly,~~ A capping agent is used

to direct TiO_2 crystal growth in a specific direction as the result of its preferential adsorption in a particular crystal plane. Other reaction parameters, such as the presence of Ti precursors, reaction time, temperature and the type of solvent, can influence the exposure of a particular crystal facet [31].

The TiO_2 {101} facet is one of the most common crystal facets in the anatase phase due to its low surface energy. Nevertheless, the truncated octahedral bipyramid with eight {101} facet and two {001} facets is found to be the most common crystal shape of anatase in the nature-based Wulff construction [29,30]. Hence, many efforts have been made to develop synthetic routes for the formation of TiO_2 that show only a {101} facet. One of the earliest approaches was to slow the reaction rate, which can be achieved by using Ti(III) as the precursor rather than Ti(IV) [42–45]. In this approach, Ti(III) is considered to be oxidized to Ti(IV) before it undergoes hydrolysis under hydrothermal conditions. Consequently, this would significantly slow the overall reaction rate due to the lack of dissolved oxygen. This approach was successfully applied by Hosono *et al.* when they prepared anatase TiO_2 nanooctahedra with approx. 100% exposure of {101} facets using $TiCl_3$ as the precursor in the presence of sodium dodecyl sulfate (SDS) as a capping agent [42]. Based on the result, it was also suggested that SO_4^{2-} from SDS was responsible for the formation of an equilibrium crystal shape. This was proven by the formation of slightly different slender pyramidal morphology when H_2SO_4 was used instead of SDS. In another report, a similar approach of utilizing $TiCl_3$ as the Ti precursor was also reported in the hydrothermal synthesis of TiO_2 with {101} facet [44]. In this approach, H_2O_2 was added as an oxidizing agent to produce the intermediate $Ti(O_2)_3^{2-}$. In contrast, HCl was used to suppress the formation rutile TiO_2 phase and to induce the crystal growth into [101] direction. As a result, pyramidal anatase TiO_2 with 100% exposure of {101} facets could easily be obtained.

Furthermore, highly exposed (101) facet of TiO_2 nanocrystals with octahedral morphology could also be obtained by transforming amorphous one-dimensional TiO_2 nanofiber via hydrothermal method at 160 °C [46]. Based on the result, it is reported that such an approach was able to produce uniform octahedral TiO_2 nanoparticles with high specific surface area (SSA) that exhibit {101} facet and a small percentage of {100} facet predominantly. Furthermore, Wu and co-workers have also successfully synthesized single-crystalline anatase TiO_2 nanobelts with a high degree of surface exposure of (101) facet by a hydrothermal transformation of TiO_2 powder in concentrated NaOH aqueous solution [47]. It was found that the as-prepared (101)-exposed TiO_2 nanobelts exhibited a lower rate of excitons recombination due to the significant enhancement in charge mobility, fewer localized recombination zones due to the reduction of unpassivated surface states, and improvement in the ability to trap photogenerated electrons. In another report, two-dimensional TiO_2 with a high percentage of {101} facet could also be obtained by converting both crystalline and amorphous TiO_2 via the chimie-douce (soft chemistry) method. For instance, Peng and co-workers have successfully converted commercial anatase TiO_2 powder into two-dimensional (101)-exposed anatase TiO_2 nanosheet [48]. Based on their results, it is believed that the bulk anatase crystals were able to be initially dissolved into several zigzag titanate chains building blocks in highly basic conditions, which could then be recrystallized back into the lepidocrocite structure where the exposure of (101) surface is mostly preferred. Figure 2 shows a schematic illustration for the conversion pathway of commercial bulk anatase to two-dimensional (101)-exposed anatase TiO_2 nanosheet.
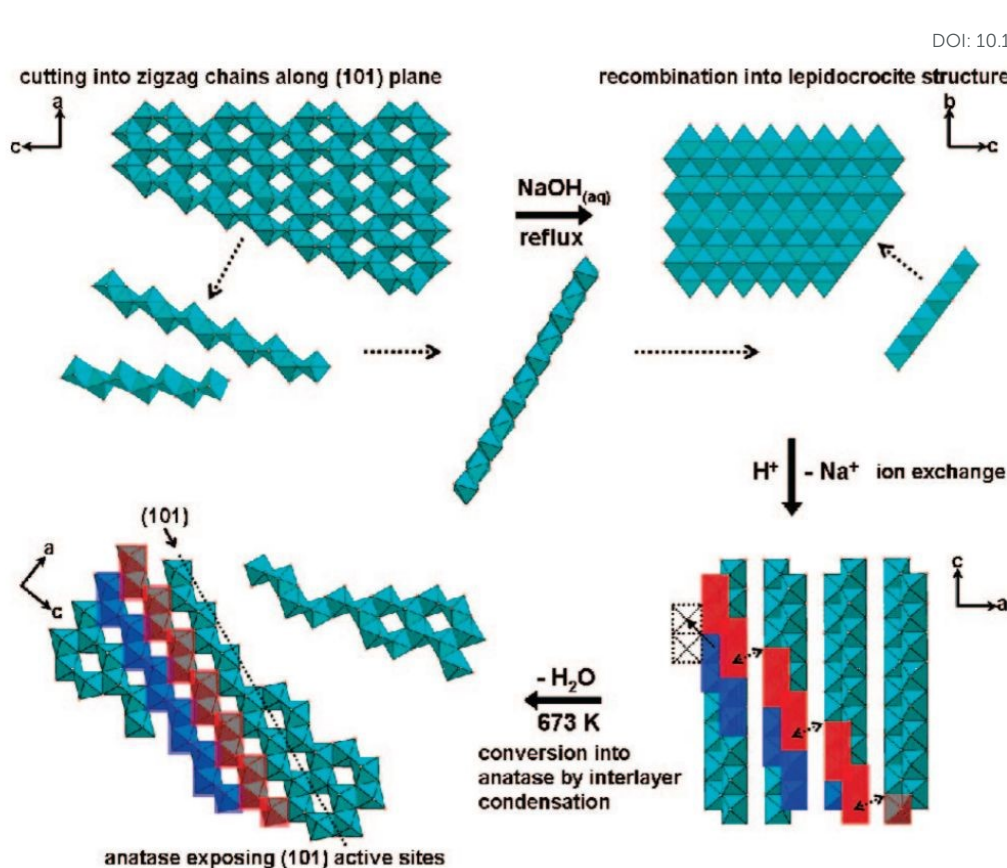
Figure 2. Schematic illustration of the conversion pathway of commercial bulk anatase to two-dimensional (101)-exposed anatase TiO_2 nanosheet in the chimie-douce method. Reprinted with permission from [48]. Copyright 2008, American Chemical Society.

Another approach that can be used to prepare two-dimensional TiO_2 nanocrystals with high exposure {101} facets is by selecting the appropriate capping agent. For example, Yang and co-workers were able to develop a robust and straightforward synthetic protocol for TiO_2 nanoleaves using a hydrothermal method at 140°C where titanium(IV) isopropoxide and triethylamine (Net_3) are as Ti precursor and capping agent, respectively [49]. Based on the result, the as-prepared TiO_2 nanoleaves were able to be self-assembled into facet-selective two-dimensional stacking structure along the [101] plane using Zn(II)-porphyrin and the bidentate bipyridine. Recently, two-dimensional NTA was also successfully transformed into anatase TiO_2 nanostructures with up to 95% exposure of {101} facet using a solvothermal method where tert-butyl alcohol as the solvent [50]. According to the report, it is found that the percentage of {101} facet of the as-prepared TiO_2 nanocrystals was proportional to its photocatalytic ability in hydrogen production. This superiority in catalytic performance was believed primarily due to the ability of a TiO_2 {101} facet to serve as reduction sites with an enriched electron population.

In the literature, fabrication of two-dimensional TiO_2 nanostructures with a high exposure of {001} facets is by far the most exploited approach due to their high surface energy. In most cases, the synthesis of such material is carried out by preventing the crystal from growing in [101] direction at the naturally occurred TOB shape according to Wulff construction. This can be achieved by making sure the crystal growth is carried out under the non-equilibrium condition at controlled kinetically regime [51,52]. In general, the TiO_2 crystal nucleus would initially evolve as a TOB seed. Under equilibrium condition, TiO_2 [33] facets would rapidly be

diminished as the crystal prefers to grow into thermodynamically stable TOB with predominately {101} facet. This is mainly because {101} facet has significantly lower surface energy than {001} facet. Under non-equilibrium conditions, high surface energy {001} facets could be stabilized, resulting in the formation of a metastable two-dimensional TOB crystal with increased exposure of {001} facets. Figure 3 presents the schematic illustration for TiO_2 crystal evolution in both equilibrium and non-equilibrium conditions.
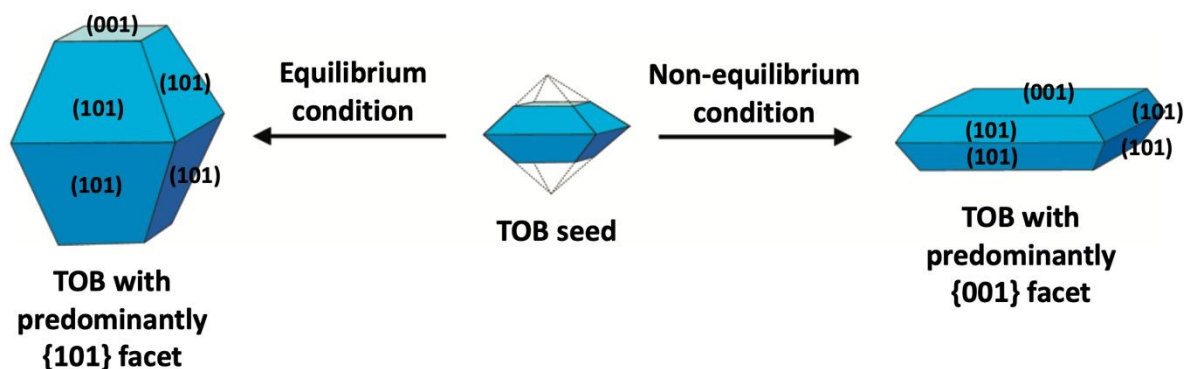

Figure 3. Schematic illustration of TiO_2 crystal evolution under equilibrium and non-equilibrium conditions.

Traditionally, a non-equilibrium condition during TiO_2 crystal growth could be kinetically achieved by controlling the temperature and ramping rate during the reaction. For example, Ahonen and co-workers were able to create a non-equilibrium condition by carrying out rapid heating and quenching of titanium(IV) isopropoxide at high-temperature (1200 °C) gas phase thermal oxidation [53]. Based on the result, it was found that such a condition was able to form a well-faceted anatase TiO_2 particle with predominant exposure of {001} facet. In another report, similar rapid heating and quenching approach was also carried out using $TiCl_4$ as the precursor [54]. Here, the thermal oxidation process was done by liberating Ti precursor vapor using argon bubbles and mixed with high-rate oxygen stream where it was subsequently subjected to high temperature (1300 °C), which results in the formation of decahedral single-crystalline TiO_2 particles with up to 40% exposure of {001} facet. Both thermal oxidation temperature and its ramping rate were crucial in this synthetic method. A high exposure of {001} could only be achieved when the annealing temperature was above 500 °C with a ramping rate above 16 °C min^{-1} [55,56]. This synthetic approach also known resulted in the formation of rutile TiO_2 phase as a byproduct [53]. This method has been widely considered unsuitable for the scalable industrial production of such products.

Many recent studies have considered the influence of various reaction dynamics for the synthesis of TiO_2 crystal with high exposure of {001} facet in both aqueous and non-aqueous liquid phases system. It has been shown that selecting a suitable titanium precursor, reaction temperature, pressure and solvent is important. The introduction of capping agents is essential to control the crystal nucleation [21,28]. Among these factors, the type and amount of capping agent are considered as the most crucial contributing parameters in ensuring the high exposure of {001} facet in TiO_2. This is primarily due to the kinetics of crystal growth is exponentially proportional to the crystal surface energy [51]. Typically, the specific surface energy of a crystal can be enhanced or reduced by selective adsorption of a capping agent on that particular crystal facet [30]. As a result, the presence of a specific capping agent can significantly influence the final shape of the crystal. For the case of TiO_2 with high exposure of {001} facet, fluorine-based capping agent has been widely utilized due to their strong preferential interaction and ability to stabilize {001} facet [5]. During the past several years, different types of fluorine-based

capping agents, such as HF, NH_4F, NaF, and [bmim]-[BF_4], have been effectively used to synthesize TiO_2 with high exposure of {001} facet [5,57–60]. Besides, the utilization of fluorine-based Ti precursors, such as TiF_4 and $TiOF_4$, have also been reported to be able to produce TiO_2 with high exposure {001} facet due to the simultaneous *in-situ* generation of F^- species [61,62]. Furthermore, a study by Liu and co-workers revealed that the variation in the degree of co-exposure for both {101} and {001} facets could also be simply controlled by the ratio of HF/H_2O during the solvothermal reaction [63]. Based on the result, the percentage of {001} facet exposure was found to be proportional to the concentration of HF. Using this synthetic approach, two-dimensional TiO_2 nanosheets with ≈92% exposure of {001} facet were successfully fabricated and proven to exhibited exceptional ability as an antibacterial agent due to the presence of {101}/ {001} surface heterojunction. Figure 4 shows SEM and TEM images of the as-prepared TiO_2 nanocrystals with different degree of {001} facet exposure prepared at various HF/H_2O ratio.
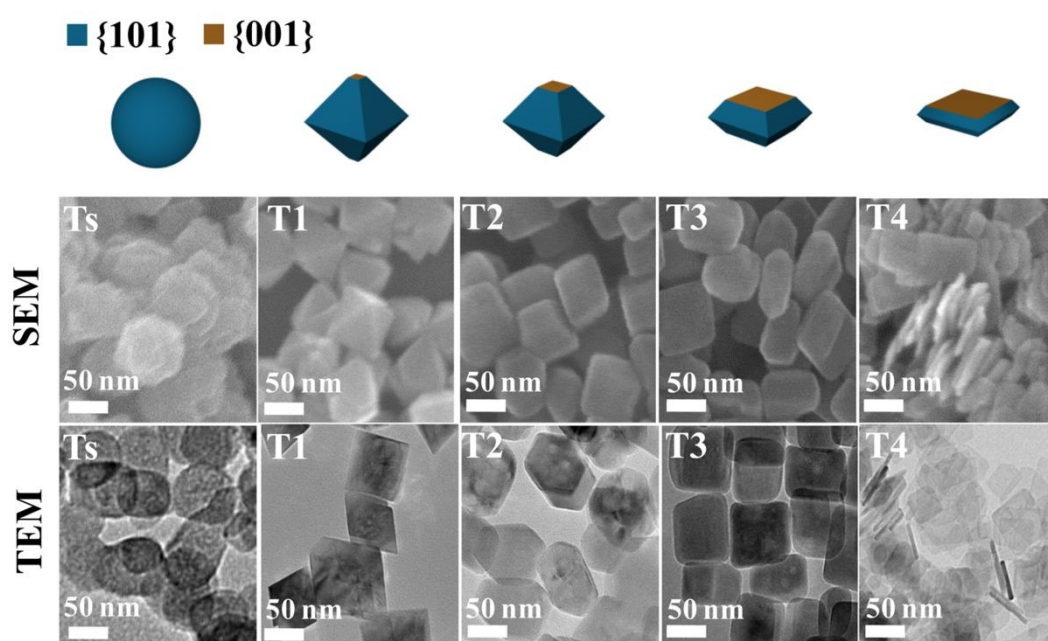

Figure 4. SEM and TEM images of TiO_2 nanocrystals with different degrees of the {001} facet synthesized at various ratios of HF/H_2O. Reprinted with permission from [63]. Copyright 2017, American Chemical Society.

Additionally, a fluorine-free hydrothermal route with K-titanate nanowires and urea as the precursors was also introduced for the synthesis of two-dimensional TiO_2 nanostructures with {001} facet [64]. In this synthetic approach, it was reported the carbonate ions resulted from the decomposition of urea were found to be responsible for the formation of a high percentage of {001} facet (60%). In other reports, other inorganic species such as Cl^- and SO_4^{2-} anions, were also reported to be sufficient for directing the formation of TiO_2 nanocrystals with high exposure of {001} facet [65,66]. Recently, organic-based capping agents have also been explored for a similar application. For instance, Khalil and co-workers have also reported that an amine-based capping agent, i.e., DETA, could also be utilized to expose {001} facet during the hydrothermal synthesis of TiO_2 with spindle-like morphology [33,67]. In another study, Chen *et al.* successfully fabricated hierarchical sphere microstructures comprising of self-assembled two-dimensional ultrathin TiO_2 nanosheet with nearly 100% exposure of (001) facet using a mixture of isopropyl alcohol and DETA as capping agent [10]. Recently, a combination of HF

and polymer-based capping agents, i.e. poly(vinylpyrrolidone) (PVP), has also been reported to be able to be utilized for the synthesis of TiO_2 nanomosaics comprising two-dimensional TiO_2 with a high percentage of exposure for {001} facet [68]. In this report, it was believed that large and bulky polymeric PVP molecules could serve not only as the linker between TiO_2 nanosheets, but also prevent them from stacking together along the *c*-axis.

2.2. Monolayer titanate

Since 1998, Sasaki *et al.* [17] have studied the single layered nanosheets prepared by chemical exfoliation of lepidocrocite-like titanate, in which the solid-state reaction was the main method used to synthesis the parent compound at that time. [69]

Since the reaction occurs in solid state, high temperature process (800-1500 °C) is usually required to induces the reaction of solid precursors [70]. To ensure a uniform reaction, crushing and grinding are usually deployed with mortar and pestle to produce an intimate mixture of precursors while ball milling could be used for larger quantity. To help with the homogenisation, a small amount of solvent such as alcohol or acetone can be added, in which it will evaporate after the precursors is perfectly mixed [70]. Instead of using additional solvent, pelleting could be deployed as an alternative to produce a good contact between precursors. The rate of solid-state reaction could be controlled by adjusting the temperature and by considering certain properties of the precursor such as surface area, its reactivity, and morphology. To increase the reactivity, a molten salt is often used as an additive as well as a solvent [71].

Common solid-state reaction of titania and alkali salt precursors, such as $CsNO_3$, Cs_2CO_3, and K_2CO_3 often results in a fibrous (monoclinic) titanate structure. In 1987, Grey *et al.* [69] discovered a new type of titanate compounds using a non-stochiometric reaction, where the resulting product has a layered structure, that is lepidocrocite-like (orthorhombic) titanates. Figure 5 shows the crystal structures and scanning electron microscopy (SEM) images of the fibrous and lepidocrocite-like titanate compounds.
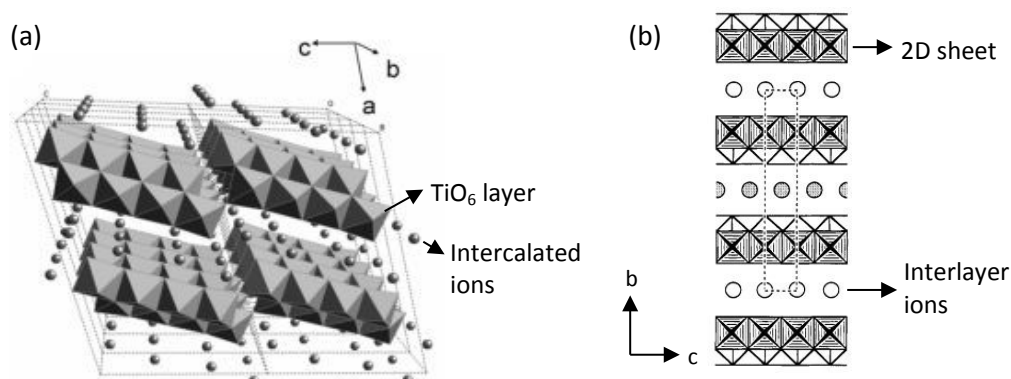
(c)

(d)

20 μm

Figure 5. (a) Crystal structure of fibrous-like titanate (monoclinic) [72]; (b) Crystal structure of lepidocrocite-like titanate (orthorhombic) viewed down along the a-axis [73]; (c) FESEM image of fibrous-like titanate [73]; (d) FESEM image of lepidocrocite-like titanate [74]. Panel (a) adapted with permission. [72] Copyright © 2010, American Chemical Society. Panel (b, c) adapted with permission. [73] Copyright © 1995, American Chemical Society. Panel (d) adapted with permission. [74] Copyright © 1998, American Chemical Society.

In the Grey *et al.* method, a molar ratio of TiO_2:$CsNO_3$ was mixed around 1:2.8-3.2 followed by heating at 800-1050 °C for 0.5-20 hours producing a white powder of lepidocrocite-like caesium titanate with the chemical formula of $Cs_xTi_{2-x/4}\square_{x/4}O_4$, where x is about 0.61-0.65 and

$\square$ represents a titanium vacancy. The procedure has been further developed by Sasaki *et.al.,* who used Cs_2CO_3 and TiO_2 with molar ratio of 1:5.3 exhibiting lepidocrocite-like lamellar sheets [73]. Besides caesium-based precursor, Sasaki *et al.* also utilised Li_2CO_3 and K_2CO_3 in place of Cs_2CO_3 for the reaction with titania powder [75]. The reaction of Li-K-based titanates can be enhanced by K_2MoO_4 molten flux process, which acts as an excellent heat transfer medium. The slow-cooling procedure in the flux process yields in a very large nanosheets up to 30 microns while the solid-state reaction typically produces ≈ 0.5-1 microns [76,77].

Layered lepidocrocite-like titanate needs to be exfoliated to produce monolayer nanosheets. Sasaki *et al.* showed a facile two-step ion-exchange method to exfoliate the nanosheets. Firstly, the interlayer caesium or potassium ions were etched with acid and replaced by H^+ ions. For complete removal of alkali ions, a repeated acid treatment with a fresh solution was required in which 98% of alkali ions were removed after three daily cycles [72]. As a result, lepidocrocite-like titanate with a high cation-exchange capacity was produced after the acid ion-exchange reaction resembling the smectite clay like behaviour.

Secondly, the bulky ions exchange with TBA^+ or TMA^+ ions was conducted to assist complete exfoliation of protonated layered titanate. The properties of the resulting compounds were similar to smectite clay such as montmorillonite, hectorite, and saponite, in which the basal spacing could be expanded (swollen) by the intercalation of guest molecules. Depending on the concentration of bulky ions, the titania nanosheets can be in intercalated, exfoliated, or osmotic-swelling states [17] as shown in Figure 6. An extensive study on the exfoliation of

nanosheets has been conducted by Sasaki *et al.* [17] By controlling the mole ratio of TBA$^+$ to H$^+$, the state of titania nanosheets can be adjusted from intercalation → exfoliation → swelling. For caesium-based titania nanosheets, the intercalation state occurs when the ratio of TBA$^+$/H$^+$ is less than 0.5 as examined by SAXS. As the number of bulky ions increases the interlayer spacing of nanosheets increases leading to infinite interlayer spacing inducing exfoliation. The fully exfoliated state occurs within the ratio of TBA$^+$/H$^+$ of 1-5. When the ratio of TBA$^+$/H$^+$ exceeds 5, a multilayer arrangement of lamellar sheets occurs exhibiting diffuse double layer through osmotic swelling. During osmotic-swelling state, the interlayer spacing become smaller leading to sheets coagulation as the number of ions increases. One must note that, the ratio of TBA$^+$/H$^+$ varies for each types of nanosheets depending on the stoichiometry and charge density of layered compounds [75,78,79]. This chemical exfoliation method may produce very large nanosheets if gentle stirring or shaking is applied during the exfoliation process [75].
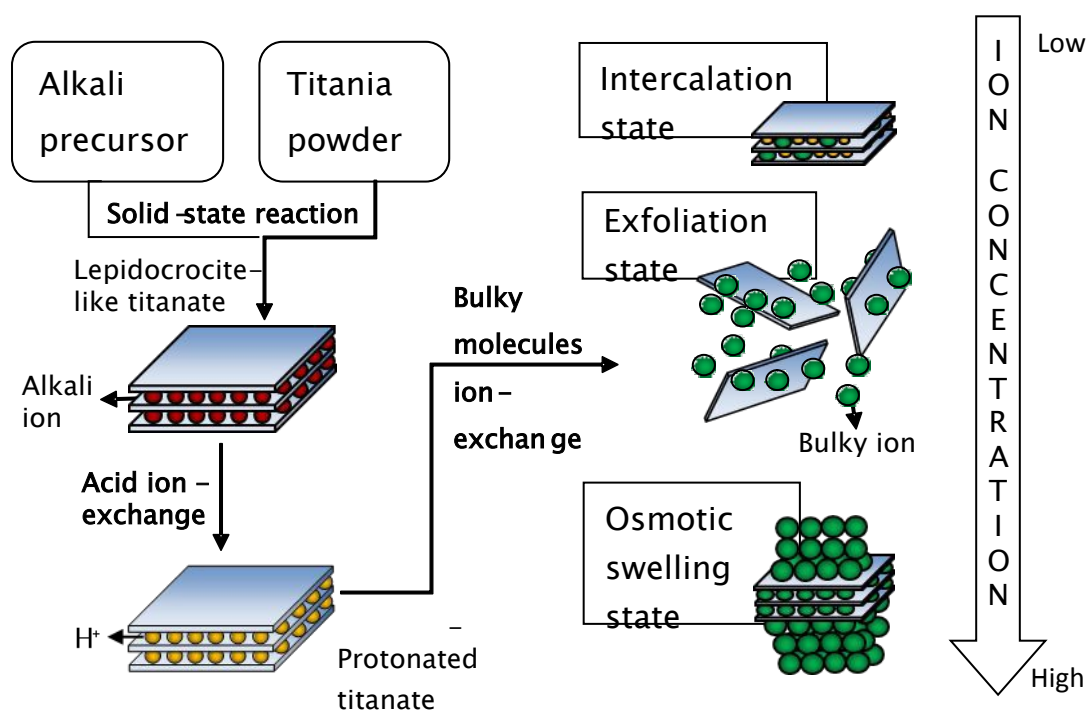
Figure 6. Schematic representation of synthesis of single-layer titania nanosheets via chemical exfoliation process. [80] Copyright © 2017 IOP Publishing.

Besides the chemical exfoliation method, the exfoliation can be conducted by mechanical approaches such as supercritical fluid exfoliation [81] and ultrasonication assisted ion-exchange [82]. High energy jets created by bubbles implosion during ultrasonication break up layered nanosheets in a relatively short time although it also reduces the lateral size of nanosheets. Meanwhile, the supercritical fluid method utilises the fluid expansion to exfoliate the nanosheets. A supercritical fluid is any compound at a temperature and pressure above its critical point, where intermediate phase, which can effuse through solids like a gas and dissolve materials like a liquid, occurs. At the beginning, the layered nanosheets are intercalated by the supercritical fluid. In this state, the exfoliation can easily occur by applying the thermal stress to the intercalated nanosheets. However, the exfoliated nanosheets may be restacked upon

cooling down, hence faster colling rate is preferable. The highest yield of exfoliated nanosheets by this method, however, was estimated only 10%. [81]

While the chemical exfoliation method uses a top-down approach from precursors synthesized by a solid-state reaction, other researchers synthesised single layered nanosheets using bottom-up approaches such as electron beam deposition (EBD) of titania and oxygen atoms under ultra-high vacuum [83] and sol-gel method [18,84]. Ti was deposited by e-beam deposition on (1×2)-Pt(110) at room temperature ($pO_2 = 1x10^{-4}$ Pa) followed by post-annealing treatment at 700 K and cooling down in oxygen ($pO_2 = 1x10^{-4}$ Pa), resulting in titania nanosheest with 3.9×1.6 nm lateral size [83]. A sol-gel solution of titania nanosheets can be synthesised by reacting the titanium precursor (i.e., TiF$_4$ and (NH$_4$)$_2$[TiO(C$_2$O$_4$)$_2$]) with an aqueous solution of KOH or NaOH. The resulting product was a small multi-layered nanosheets hence a bulky molecule such as TBAOH or TMAOH was still required to exfoliate the nanosheets [85,86]. On the contrary, a sol-gel synthesis of TIP with the large excess of aqueous bulky molecule solution of TMAOH exhibited a high yield of diamond or rhombic shaped monolayered nanosheets [18]. The bulky molecule served as the reactant for acid-base reaction with titanic acid as well as providing enough ionic charge to maintain the exfoliation of nanosheets. Compared to the chemically exfoliated nansoheets, the sol-gel synthesis usually produces a relatively small nanosheets with less than 50 nm in lateral size.

Ban *et.al.* [87] has further developed the sol-gel synthesis by using organic ligand (e.g., triethanolamine and lactic acid) to form a titanium complex hence retarding the nucleation of titania nanosheets while promoting growth in lateral direction. This method created a ≈100 nm diamond shaped titania nanosheets after several days of reaction in autoclave. However, the organic ligand may also cause the restacking of nanosheets during evaporation hence it should be removed by dialysis. The Ban's sol-gel synthesis of large nanosheets is illustrated in Figure 7.
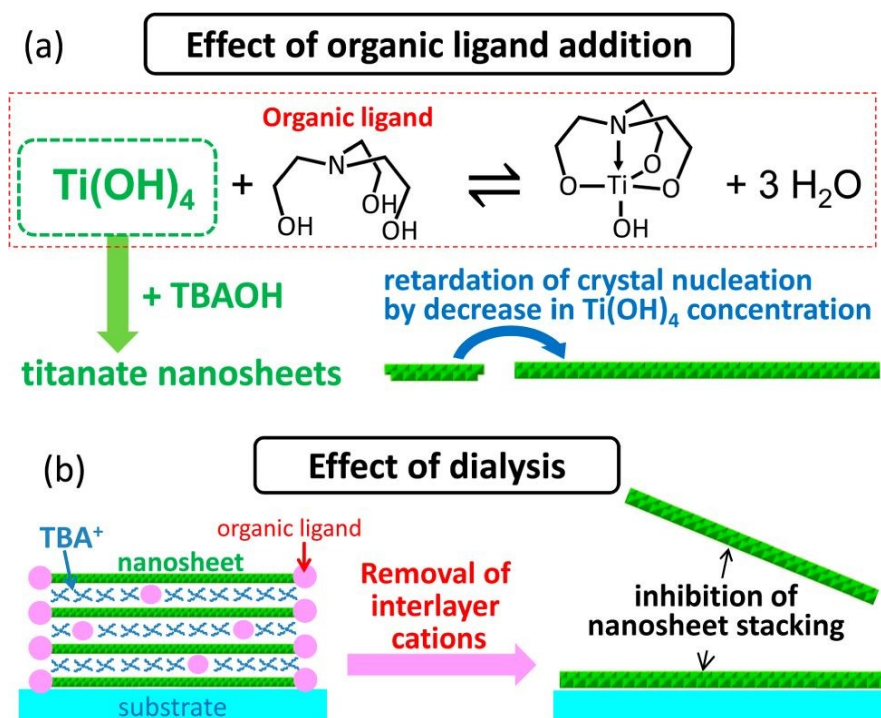
Figure 7. The illustration of (a) the effect of the organic ligand in crystallisation of the titania nanosheets and (b) inhibition of nanosheets restacking by dialysis. [87] Copyright © 2015, American Chemical Society

The need to confine the growth of titanate in the lateral dimension has been developed by another group. Sol-gel synthesis at hydrophobic/hydrophilic (i.e., hexane/ice) interface can be deployed to create large nanosheets, as illustrated in Figure 8 [84]. These nanosheets contain of several small nanodiscs with ≈5 to 15 nm in lateral size, which are agglomerated horizontally. The single layered nanosheets structure was confirmed by atomic force microscopy (AFM) whereas the nanosheets are only ≈0.5-1 nm in thickness. After hydrolysis by HCl, the anatase TiO_2 structure was formed as characterised by X-ray diffraction (XRD). A schematic of the synthesis route to TiNS is outlined in Figure 9 and it is summarized in Table 1.
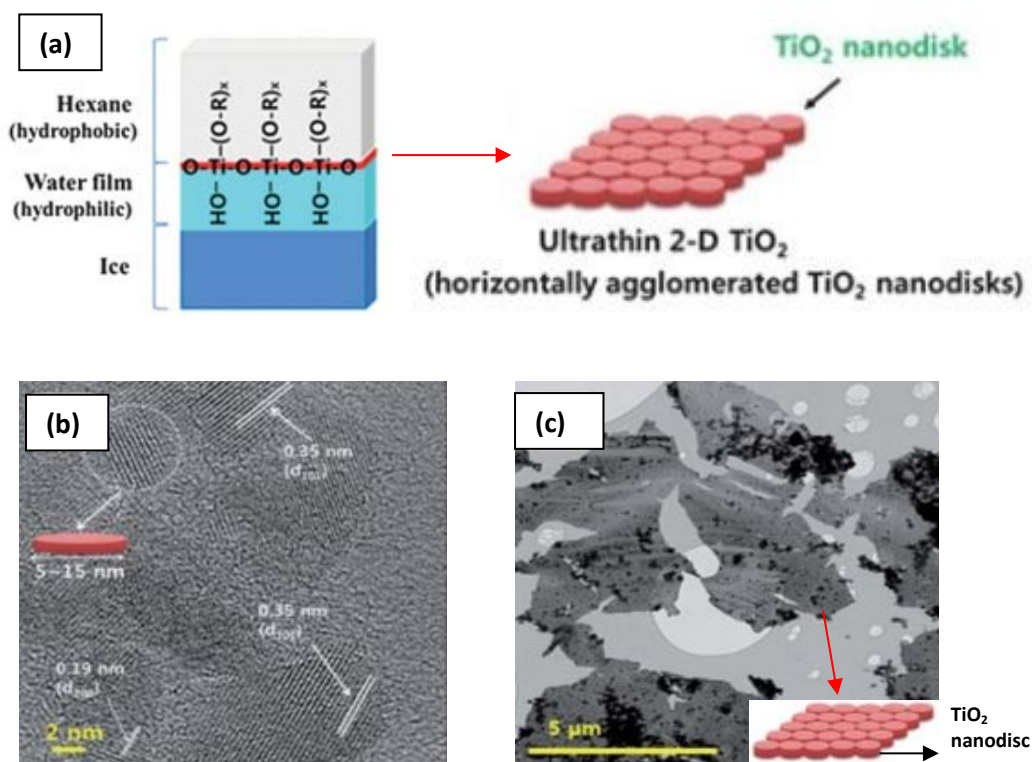

Figure 8. (a) Schematic illustration of 2-D TiO_2 formation on hexane/ice interface [84]. TEM images of a nanosheet consisting of horizontally agglomerated TiO_2 nanodiscs [84]: (b) HR-TEM image of nanodiscs, (c) TEM image of nanosheets. Reproduced from Ref. [84] with permission from the Royal Society of Chemistry.

Nanoscale Advances Accepted Manuscript

Table 1. Summary of synthesis methods for single-layered titania nanosheets.

Top-down approach				
Solid-state reaction				
Synthesis of layered nanosheets	**Exfoliation method and its additive**	**Chemical formula**	**Lateral size**	**Ref.**
$Cs_2CO_3 + TiO_2 \rightarrow Cs_xTi_{2-x/4}\square_{x/4}O_4$ (x ≈0.7; $\square$ = titanium vacancy) Reaction at 800 °C for 20 h (2 times)	Ion-exchange at 25 °C for 2 weeks by 0.00825 to 0.0825 mol L^{-1} aqueous solution of (tetrabutylammonium hydroxide) TBAOH	$Ti_{0.91}O_2^{0.36-}$	≈0.1-1 µm	[17]
$Cs_2CO_3 + TiO_2 + MgO \rightarrow Cs_xTi_{2-x/2}Mg_{x/2}O_4$ (x ≈0.7) Reaction at 800 °C for 1 h followed by 2 times heating at 950 °C for 20 h	Ion-exchange at 50 °C for 1 week by 5 wt% aqueous solution of TBAOH or (tetramethylammonium hydroxide) TMAOH	$Ti_{0.825}O_{1.825}^{0.35-}$	≈0.1-1 µm	[88]
$K_2CO_3 + TiO_2 + Li_2CO_3 \rightarrow K_xTi_{2-x/3}Li_{x/3}O_4$ (x ≈0.8); (with K_2MoO_4 as flux melt) Reaction at 1200 °C for 10 h followed by slow cooling (4 °C h^{-1}) until it reach 950 °C	Ion-exchange at 25 °C for 2 weeks by 0.0125 to 0.025 mol L^{-1} aqueous solution of TBAOH or TMAOH	$Ti_{0.87}O_2^{0.52-}$	0.5-2 µm; average ≈1 µm for TBAOH and 10-30 µm for TMAOH	[75]
$Na_2CO_3 + TiO_2 \rightarrow Na_2Ti_3O_7$ Reaction at 900 °C for 24 h	Ion-exchange by methylamine at 60 °C for 6 d followed by propylamine at 60 °C for 6 d	$Ti_3O_7^{2-}$	≈0.1-1 µm (rectangular)	[89]
$Cs_2CO_3 + TiO_2 \rightarrow Cs_xTi_{2-x/4}\square_{x/4}O_4$ (x ≈0.7; $\square$= titanium vacancy); Reaction at 800 °C for 20 h (2 times)	Ion-exchange by TBA$^+$ ion assisted with ultrasonication (60-300 W, 2-30 min)	$Ti_{0.91}O_2^{0.36-}$	≈0.1-0.2 µm	[82]

$K_2CO_3 + TiO_2 + Li_2CO_3 \rightarrow K_xTi_{2-x/3}Li_{x/3}O_4$ (x ≈ 0.8) (with K_2MoO_4 as flux melt) Reaction at 927 °C for 10 h (Spontaneous cooling)	Supercritical DMF exfoliation (400 °C, 15 min)	$Ti_{0.87}O_2^{0.52-}$	$\approx 5\text{-}20$ μm	[81]

Sol-gel followed by ion exchange

Synthesis of layered nanosheets	Exfoliation method and its additive	Chemical formula	Lateral size	Ref.
$(NH_4)_2[TiO(C_2O_4)_2] + KOH \rightarrow$ $K_{1.1}H_{0.9}Ti_2O_5\cdot2.6H_2O$ (1 day, 22–80 °C)	Ion-exchange by aqueous solution of TBAOH at 22 °C	$Ti_2O_5^{2-}$	$\approx 10\text{-}20$ nm	[85]
$TiF_4 + NaOH \rightarrow Na_{0.8}Ti_{1.8}\square_{0.2}O_4 \cdot yH_2O$ (y <1.17) (3 days, 22 °C)	Ion-exchange by aqueous solution of TBAOH at 22 °C	Not available	$\approx 2\text{-}5$ nm	[86]

Bottom-up approach

Method	Chemical formula	Lateral size	Ref.
Reflux of Ti(IV)isopropoxide (TIP) + aqueous solution of tetramethylammonium hydroxide (TMAOH); (5 min – 24 h, 100 °C)	$(TMA)_xTi_{2-x/4}\square_{x/4}O_4$ (x ≈ 0.7)	Diamond shape with diagonal length (27.3, 19.1) nm to (7.7, 5.5) nm.	[18]

TIP + organic ligand (e.g., triethanolamine or lactic acid) + tetrabutylammonium hydroxide (TBAOH) heated in autoclave at 80 °C for 1-7 days followed by dialysis with water for 2 days	$(TBA, H)_{0.7}Ti_{1.825}O_4 \cdot xH_2O$	Diamond shape with ≈100 nm lateral size [87]
Sol-gel of hexane + TIP + ice granule interface followed by hydrolysis with HCl	TiO_2	≈5 μm consist of 5-15 nm nanodiscs [84]
e-beam deposition on (1 × 2)-Pt(110); Ti was deposited at room temperature ($pO_2 = 1x10^{-4}$ Pa) followed by post-annealing treatment at 700 K and cooling down in oxygen ($pO_2 = 1x10^{-4}$ Pa)	TiO_2	3.9 × 1.6 nm [83]
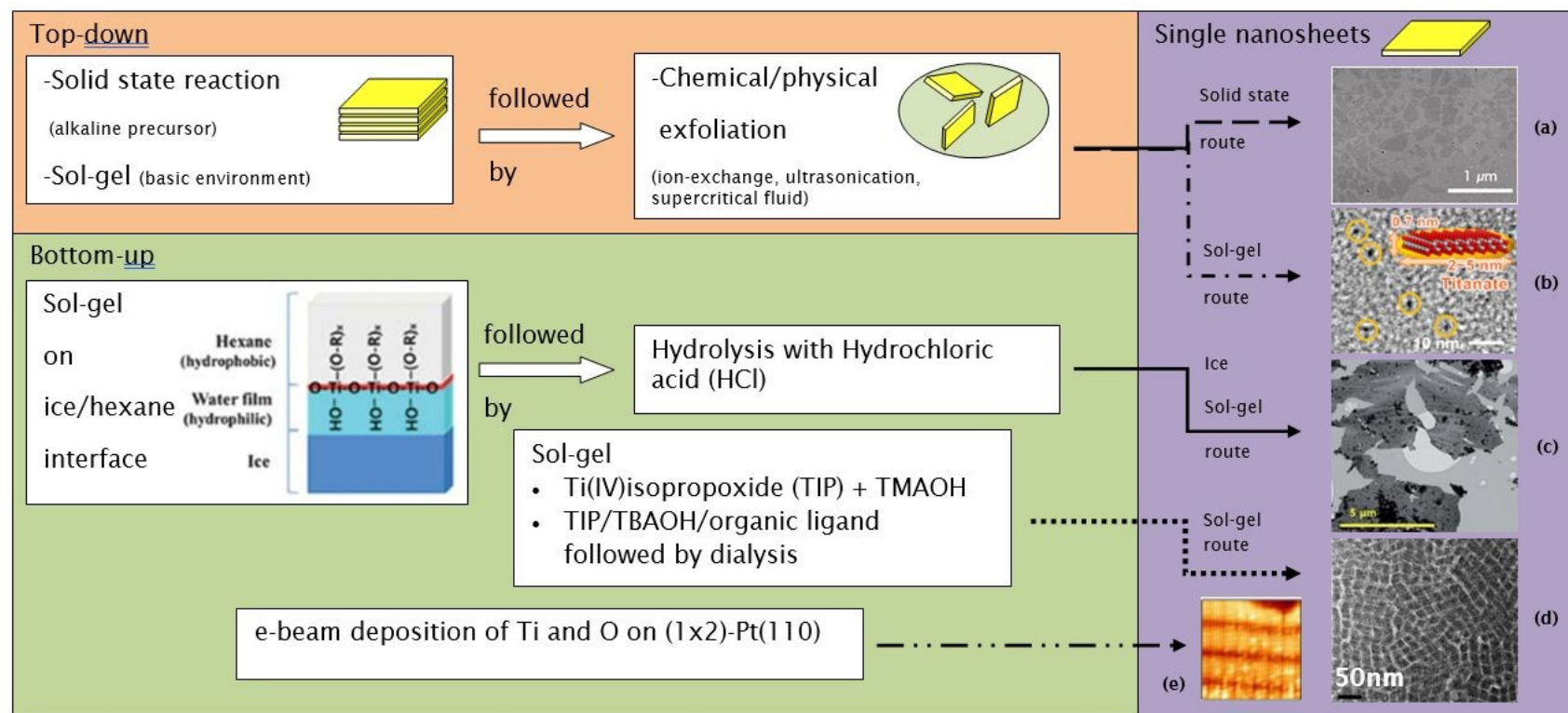
Figure 9. Several routes to synthesis single-layer titania nanosheets: **(a)** TEM image of nanosheets made by solid state route [14], **(b)** Bright-field TEM image of nanosheets made by sol-gel route [86], **(c)** TEM image of nanosheets made by ice sol-gel route [84], **(d)** TEM image of nanosheets made by sol-gel route [18], **(e)** High resolution STM image of nanosheets made by e-beam deposition route (13.6 nm × 13.6 nm; bias voltage = 0.42 V; I_T = 0.9 nA) [83]. Panel (a) adapted with permission. [14] Copyright © 2010 WILEY-VCH Verlag GmbH & Co. KGaA, Weinheim. Panel (b) adapted with permission. [86] Copyright © 2013, American Chemical Society. Panel (c) reproduced from Ref. [84] with permission from the Royal Society of Chemistry. Panel (d) adapted with permission. [83] Copyright © 2006 by the American Physical Society.

3. Properties

3.1. Physical properties

3.1.1. Exposed facets titania

Both optical and electronic properties have been widely considered as the most common direct consequences for the exposure of specific crystal facet in 2D TiO_2 nanostructures. Typically, this can easily be observed by the alteration of both bandgap and band edge location. According to recent studies, the exposure of TiO_2 {001} facet while diminishing the existence of {101} facet may contribute to the reduction of the TiO_2 optical band gap [44,90,91]. For instance, Liu et al. calculated that the optical bandgap of TiO_2 nanostructures with 5%, 60%, and 92% exposure of {001} facet was found to be 3.33, 3.29, and 3.16 eV, respectively [92]. Similar bandgap narrowing due to the exposure of {001} facet was also observed elsewhere [93,94]. According to theoretical calculation using a DFT, such reduction was most likely because {101} facet possesses a slightly higher CB than that of {001} facet [95–97]. It is also realized that such a phenomenon might also be occurred due to the presence of oxygen vacancies as a result of unique surface atomic arrangement [98,99]. Furthermore, similar band structure alteration was also observed in other high index facets. For example, using both experimental and theoretical estimations, Xu and co-workers revealed that TiO_2 with {111} facet exhibited a higher conduction band minimum in comparison to TiO_2 with {001}, {101}, and {010} facets [100]. It is believed that such a phenomenon was partially attributed due to the large percentage of undercoordinated Ti and O atoms at the surface of {111} facet. Figure 10 presents the slab model for the surface structure of TiO_2 at different crystal facets.
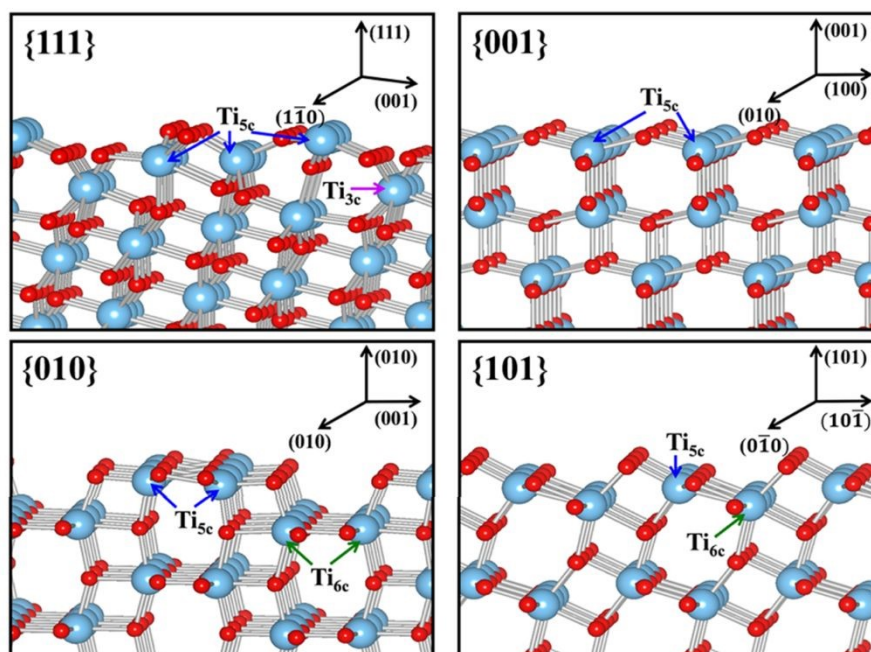
Figure 10. Slab model for the surface structures of the relaxed stoichiometric TiO_2's {111}, {001}, {010} and {101} facets. Reprinted with permission from [100]. Copyright ©2013, American Chemical Society.

Furthermore, the unique arrangement of atoms at the surface of TiO_2 due to the exposure of different facet may also influence the efficiency of charge carrier separation. Traditionally, the prevention of fast photogenerated electron-hole recombination of TiO_2 was typically done by

heterojunction or application of sacrificing agents [101,102]. However, recent studies have suggested that crystal facet engineering of TiO_2 could also be used as an effective strategy to avoid such issue [103–106]. For example, high surface energy {001} facet has been proven to exhibit superior ability in ensuring efficient separation of photoexcited charge carriers. It is believed that such a phenomenon was partly due to the presence of surface defects, e.g., oxygen vacancies, which could mediate efficient the interfacial electron transfer [21]. Additionally, a high density of undercoordinated Ti atoms and large Ti-O-Ti bond angles at the surface of {001} facet has also been considered as one of the prevalent contributors for such phenomenon [5]. Recently, the contribution of two or more co-existing facets has also been associated with the further efficient charge separation. For instance, Yu *et al.* reported that the co-exposed {001} and {101} facet was found to exhibit a synergistic effect that responsible for the enhancement of the photocatalytic activity of 2D TiO_2 nanosheet [107]. Using DFT calculation, it was revealed that the enhancement in photoactivity was primarily due to the formation of surface heterojunction between {001} and {101} facet as a result of their band alignment. This is possible since the position of CBM and VBM of {001} facet was found to be more positive than that of {101} facet [92]. As a result, the photogenerated electron tends to be thermodynamically transferred to {101}, while the hole is preferred to be moving in the opposite direction.

Another physical characteristic that may be influenced by the exposure of certain facet in 2D TiO_2 nanostructures is their capability in substrate adsorption. It is reported that specific geometric structure and atomic arrangement at the surface of a particular TiO_2 facet could affect the interaction between TiO_2 and various types of substrates, e.g., water, methanol, CO_2, or other small molecules [108–110]. One of the widely accepted rationalizations for such a phenomenon was the fact that certain facet exhibits different degrees of oxygen vacancy and undersaturated Ti coordination. For example, the surface of TiO_2's {001} facet is widely known to have 100% undercoordinated Ti-5c atoms and half saturated Ti-6c atoms. In contrast, {101} facet exhibits half of the undercoordinated Ti-5c atoms and half saturated Ti-6c atoms [31]. {001} facet is also reported to have a large stoichiometric amount of the surface hydrophilic Ti^{3+} and surface OH groups than {101} facet [111]. As a result, the sorption capacity of {001} facet for water or other polar molecules is expected to be higher than that of {101} facet. Similar superiority in the sorption capacity of {001} facet over different facets was also observed elsewhere for the absorption of $Cr_2O_7^{2-}$ and arsenic [112,113]. It is also worth noting that both specific surface area and particle size may contribute to the overall sorption capacity.

3.1.2. Monolayer titanate

The properties of chemically exfoliated titania nanosheets are related to its chemical formula in which the precursors (i.e., lepidocrocite-like titanate) have a general formula of $Cs_xTi_{2-x/4}\square_{x/4}O_4$, where x is around 0.7 and $\square$ is titanium vacancy [114,115] for caesium based and $A_xTi_{2-x/3}Li_{x/3}O_4$ where x≈0.8 for A=K (potassium) and x ≈ 0.75 for A = Rb [17]. The detailed crystal structure of of these compounds is shown in Figure 11. After alkali ions removal, the nanosheets is negatively charged with the general formula of $Ti_{0.91}O_2^{0.36-}$ for nanosheets derived from $Cs_xTi_{2-x/4}\square_{x/4}O_4$.
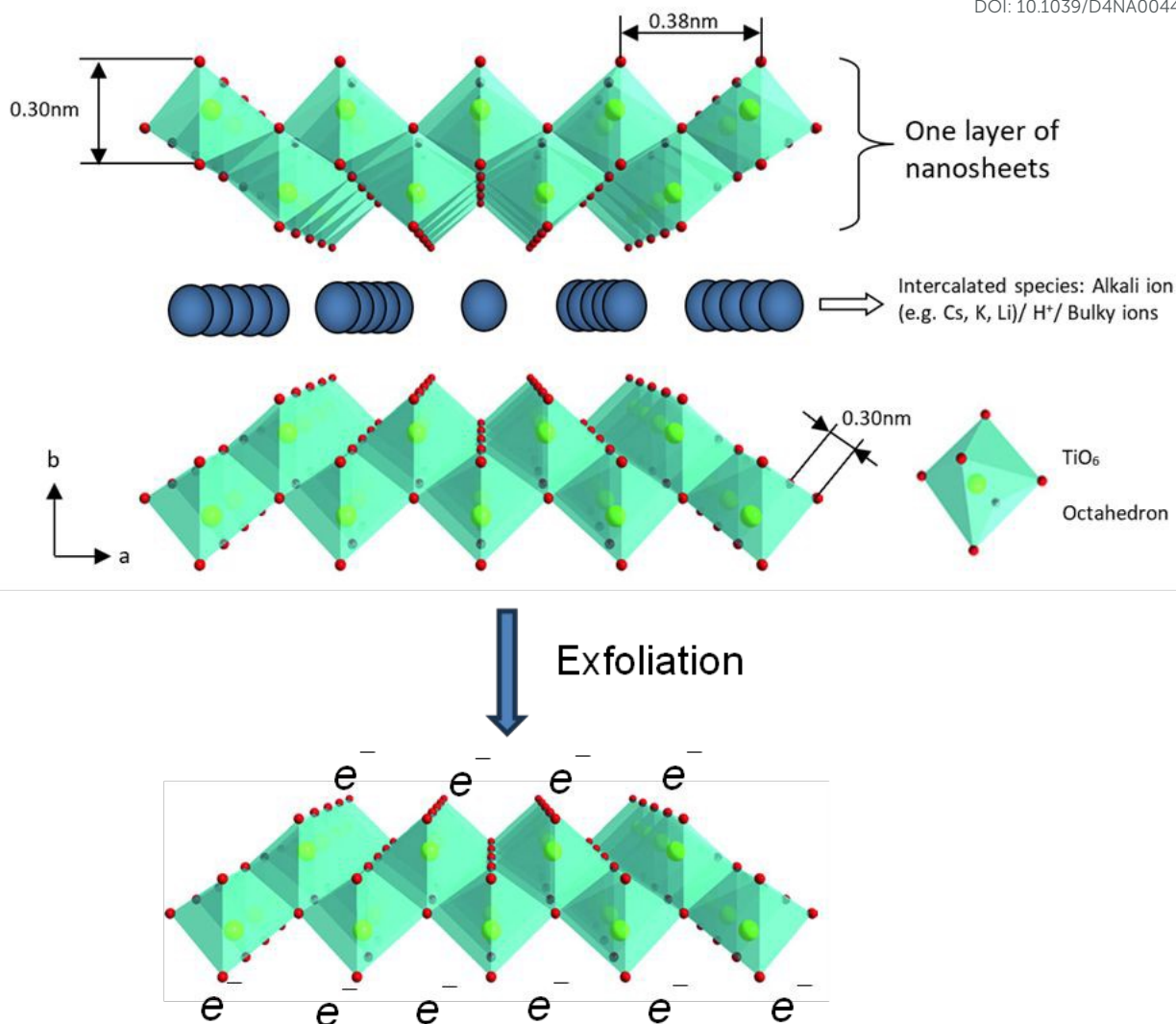
Nanoscale Advances Accepted Manuscript

Figure 11. The polyhedral representation of crystal structure of layered lepidocrocite-like titania nanosheets viewed down along the c-axis and mono-layer titania nanosheets after exfoliation. Adapted from Ref. [88] with permission from the Royal Society of Chemistry.

The absorption peak wavelength of $Ti_{0.91}O_2^{0.36-}$ nanosheets is blue shifted to around 265 nm as compared to anatase TiO_2 at 377 nm [8]. It was known that the molar absorption coefficient or molar extinction coefficient (ε) is 2.2×10^4 mol^{-1} dm^3 cm^{-1} at 265 nm [116]. This blue shift also occurs in sol-gel diamond-like titania nanosheets which has the peak around 250 nm [18]. It was concluded by both researchers that the quantum confinement significantly contributes to the optical properties of titania nanosheets especially due to the transition from 3D to 2D structure. Using spectroscopic ellipsometry, the refractive index of $Ti_{0.87}O_2^{0.52-}$ nanosheets was found to be around 2.1 at 600 nm and the extinction coefficient of a thin film (k) was nearly zero [117]. The titanate nanosheets in the structure possess diamagnetic properties which may aligned itself in 2D plane perpendicular to magnetic flux direction due to highly anisotropic magnetic susceptibility [118]. The magnetic susceptibility can be altered via UV photoreduction of Ti^{IV} to

Ti $^{IV/III}$ nanosheets, which exhibits paramagnetic properties. It changes the orientation from orthogonal to parallel direction when exposed to the magnetic field as depicted in Figure 12.
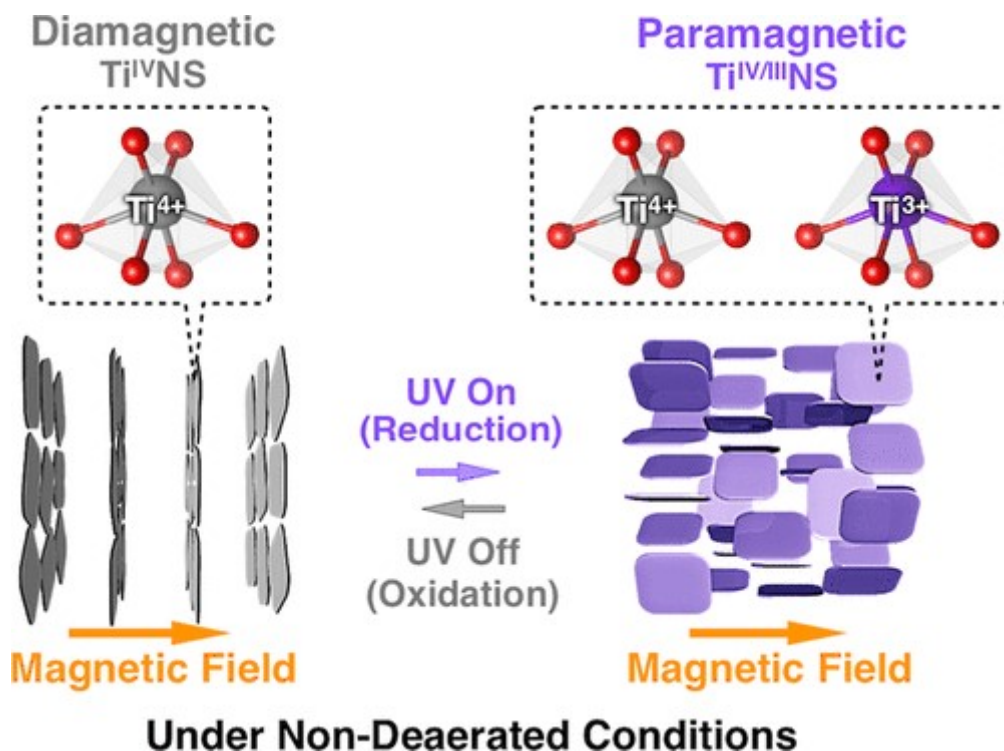

Figure 12. The orthogonal and parallel magnetic orientation switching of titania nanosheets via photoreduction and oxidation [118]. Copyright © 2018, American Chemical Society.

The electronic band gap energy of $Ti_{0.91}O_2^{0.36-}$ nanosheets was 3.84 eV as estimated by *in-situ* UV-vis spectroscopy [119], which is 0.6 eV larger than anatase titania [120]. Compared to anatase TiO_2, TiNS has slightly higher conduction band at -1.27 eV vs Ag/Ag$^+$ and significantly lower valence band at 2.53 eV vs Ag/Ag$^+$ [119]. The exfoliated titania nanosheets has larger band gap than its lepidocrocite-like titanate precursor, hence further confirming the effect of quantum confinement. Compared to the anatase TiO_2, stronger UV light is required to activate the photocatalytic capability of titania nanosheets. To overcome the large band gap, metal and non-metal doping are often introduced for narrowing the band gap. Due to a titanium vacancy in the structure, co-doping is possible for titania nanosheets [119]. One cation is to replace interlayer ions, while the other may co-substitutes Ti^{4+} in octahedral sites. Fan *et al.* [121] utilised the photocatalytic properties of titanate titania nanosheets by doping with platinum nanoparticles via photoreduction of Pt(IV) ions, which is indicated by colour changing from white to dark grey. Besides precious metal, titania nanosheets have been doped by Fe, Ni, Co, Nb, Mn ions for metal doping and nitrogen ions for non-metal doping [119]. Few studies have examined non-metal doping; exploration of co-doping by non-metal dopant should be conducted for further research.

In terms of thermal stability, monolayered titania nanosheets maintained its structure up to 800 °C before it transformed to anatase TiO_2 [119]. The stability was reduced with increasing number of stacks of the titanate layers, in which 10 stacks of nanosheets transformed into anatase TiO_2 at around 400 °C. The 2D structure limits the diffusion of atom hampering 3D formation of anatase structure. Meanwhile, the electrical conductivity depends on the relative humidity, where it increases about 5 order of magnitude from 45% to 95% relative humidity [122]. Water

molecules adsorbed on the titanate surface can bridge electrical transport in the lateral dimension.

3.2. Chemical properties

3.2.1. Exposed facets titania

The unique geometric structure and atomic arrangement at the surface of 2D TiO_2 nanostructures with certain exposed facets have also been associated with the enhancement of their catalytic reactivity. Recently, the ability to control surface and electronic properties via crystal facet engineering of 2D TiO_2 nanostructures has attracted much attention as a way to improve their performance in various applications, especially in catalysis or light-harvesting devices. It is believed that the presence of undercoordinated Ti atoms and the number of oxygen vacancies at certain crystal facet has a significant influence in dictating both the kinetic and thermodynamic of the reaction. For instance, TiO_2 with high exposure of {001} facet has been well-documented to be more reactive towards water dissociation and more effective for facilitating photoredox reactions than that of {101} facet [30,110]. In another report, Amano et al. have also reported that the performance of 2D decahedral single-crystalline TiO_2 with high exposure of {001} facet in hydrogen evolution via water splitting reaction was superior to that of commercial P25 Degussa TiO_2 powder [54]. Recently, Khalil and co-workers have also proven that the exposure of {101} facets was responsible for the enhancement in photocatalytic activity of nano Au-TiO_2 heterostructures for photodegradation of organic pollutants [33]. Based on the result, the synergistic effect between surface plasmon resonance phenomenon and the exposure of {001} feature was able to significantly increase the reaction rate by ten folds. Furthermore, they also reported that a similar enhancement in photocatalytic activity by co-exposure of TiO_2 (101) and (001) facets was also observed in photocatalytic reduction of bicarbonate using CdSe-TiO_2 nanostructures [67].

In addition to the enhancement in catalytic activity, the exposure of certain crystal facet in 2D TiO_2 nanocrystals was also reported to be responsible in the variation of catalytic selectivity. For instance, the selectivity of toluene conversion to benzaldehyde can be enhanced by simply increasing the percentage of exposure for {001} facet in two-dimensional TiO_2 nanosheet [62]. According to the report, the selectivity for the formation of benzaldehyde could be increased by up to 93% (yield 26%) by exposing 50% of {001} facet. In another report, Liu and co-workers also reported that the exposure of {001} facet could also influence the selective adsorption and photocatalytic activity towards azo dyes [123]. It was revealed that TiO_2 with low exposure of {001} facet (P25 titania, 5% of exposed {001} facet) showed a preferential photocatalytic decomposition of MO. Meanwhile, TiO_2 with high exposure of {001} favours for the degradation of MB. In literature, this selectivity was believed to be originated from the unique surface atomic configuration of {001} facet, which results in the alteration of surface characteristics such as surface charge, Lewis and Bronsted acidity, and exposed functional groups [124,125]. It is also suggested that the spatial distribution of redox sites due to the preferential separation of photogenerated charge carriers at certain crystal facet may also contribute to the aforementioned catalytic selectivity [126,127].

3.2.2. Monolayer titanate

The high reactivity of interlayer alkali metal ions such as Cs^+ and K^+ is of advantage for the ion exchange reaction with protons that facilitate the exfoliation of titania nanosheets. The cation exchange capability of chemically exfoliated titania nanosheets is beneficial in energy storage application, for example it can be used for lithiation and de-lithiation in a lithium-ion battery.

In terms of colloidal stability, a net negative charged on the titanate surface is formed after the removal of alkali metal ions, in which it is stable in basic solution with the point of zero charge at pH 8 and zeta potential of -37 mV at pH 10-13 [128]. In TBAOH or TMAOH solutions, the colloidal suspension of chemically exfoliated titania nanosheets is stable for more than 6 months. It was observed that sol-gel titania nanosheets are more stable due to smaller particle size. A stable colloidal suspension is convenient for deposition process, in which controlled deposition of titania nanosheets can be realised by Langmuir-Blodgett procedure and electrostatic layer-by-layer assembly [129]. Alternatively, an amount of titanate can be drop casted on the surface yielding in a film with cation conducting properties [130]. Electrophoretic deposition can also be performed to decorate the electrode via negative surface charge of chemically exfoliated titania nanosheets [131]. Negative surface charge also exhibited in sol-gel titania nanosheets [132]. When an electrophoretic deposition technique combines with a mechanical stimulation, a small sol-gel titania nanosheets can be inserted within titanate nanotubes creating a hierarchical structure [132]. titania nanosheets

Modification of surface functional group of titania nanosheets have been studied [128]. In an aqueous solution, chemisorbed and physiosorbed water molecule are attached to the surface of titanate leading to hydroxylated surface, where the functionalisation can be performed via this hydroxyl grouptitania nanosheets. Generally, the modification of hydroxyl group of titanate can be approached via hydrolysis with silane groups, esterification with carboxylic acid, peroxo-titanium complex formation by H_2O_2, acid-base reaction, and formation of admicelles by surfactant [133,134]. Silanisation with APTES altered the zeta potential of titania nanosheets via amino-end groups, in which the APTES-titania nanosheets has the point of zero charge at pH 6 and it is stable in acidic solution (pH < 4) [128]. Similar to titanate nanotubes which has a lot of hydroxyl groups on its surface, the chemically exfoliated titania nanosheets are also highly reactive to H_2O_2. Reaction with H_2O_2 creates titanium (IV) peroxo-complex indicated by colour transformation from white to yellow. Interestingly, the colour reverts back to white after reacting with azo dyes indicating the release of oxo group while cutting the azo dyes chain [135]. The colour transformation does not occur in sol-gel titania nanosheets, probably due to the hindrance caused by excess of bulky molecules of TMAOH. Further study is required for the formation of peroxo complexes in sol-gel titania nanosheets.

4. Applications

4.1. Exposed facets titania

In the past several years, exposing certain crystal facet in TiO_2 has emerged as a highly promising avenue for solving several challenges that hampers the efficiency of conventional TiO_2 in photocatalysis. The exposure of an unusual active crystal facet in TiO_2 has garnered significant attention as one of many potential solutions to enhance photocatalytic performance by improving light absorption and charge carrier recombination. For example, Wu and co-workers demonstrated that synthesizing rutile TiO_2 with tuneable ratio of {110} and {111} facet was evidently able to enhance photocatalytic activity in hydrogen evolution reaction [136]. A tuneable ratio of both unusual facets was achieved by using seed-mediated hydrothermal method using NaF as crystal directing agent. Based on the result, rutile TiO_2 with wholly {111} facet photocatalyst was found to exhibit the most superior photocatalytic activity towards hydrogen production under the irradiation of UV light. This was attributed to the exposure of the more reactive {111} facet.

In another report, it is reported that exposing (001) facet in anatase TiO_2 was also evidently able to provide a significant increase in photocatalytic activity of Au-TiO_2 nanocomposite in photodegradation of potent organic dye under visible light [33]. According to this work, it is evident that anatase TiO_2 with nanospindles morphology exhibited a four-time higher photocatalytic reaction rate than TiO_2 with nanocube morphology. Such enhancement in activity of TiO_2 nanospindles was believed to be due to the highly exposure of (001) facet, which responsible for improving migration and separation of the generated charge carriers. As a result, this would allow an efficient prevention of fast electron-hole recombination and lead to a better photocatalytic performance. Similar enhancements in activity for photocatalytic activity was also observed when (001) exposed TiO_2 was composited with other materials such as two-dimensional graphene oxides or CdSe quantum dots nanoparticles [67,137].

Recently, a composite of $BiVO_4$ and anatase TiO_2 with co-exposed (001) and (101) facets was also used as photoanode materials and exhibited good performance in photocatalytic fuel cell (PFC) [138]. In this study, the as-prepared photoanode was able to exhibit a considerably high photoelectrochemical response with current density of 29.8 $\mu A/cm^2$ (at 0.8 V vs. NHE) under such a low-intensity illumination of 13 W LED light. Additionally, the photoanode was able to generate electric power of 0.00232 mW/cm^2 using rhodamine B (RhB) as fuel. It is believed that such enhancement was originated from the ability of co-exposed (001) and (101) facets in TiO_2 to form an internal surface heterojunction in addition to the already existing external interfacial heterojunction between $BiVO_2$ and TiO_2. As a result, this would allow a further enhancement and efficient distribution of photogenerated charge carriers.

The exposure of unusual crystal facet in TiO_2 has also attracted considerable attention in recent years for the application of solar energy harvesting, particularly in photovoltaic solar cells. Typically, solar cell relies primarily upon efficient light absorption, charge separation, and transport to maximize energy conversion efficiency. To serve such purposes, mesoporous semiconducting materials such as TiO_2 is often used as both support light absorption layer and ETL. Nevertheless, commercial and conventional TiO_2 often suffers from poor conductivity, inefficient electron mobility, and low diffusion rate of carrier, leading to low power conversion efficiency. Crystal facet engineering in TiO_2 presents an intriguing avenue for enhancing the performance of solar cells. The recent surge in research elucidates the potential of exposing certain facet in TiO_2 to revolutionize solar cell technology through their exceptional properties. For instance, Qaid et al. reported that TiO_2 nanocrystals with exposed {001} facet prepared with facile HF- and NaF-mediated hydrothermal method exhibited a significant improvement in performance for DSSC[139]. Additionally, similar enhancement in performance was also observed when {001} facet dominant TiO_2 nanoparticles were used as ETL in $CH_3NH_3PbI_3$ perovskite solar cells[140]. According to the experiment, it is evident that the exposure of TiO_2's {001} facet was responsible for the enhancement of electron injection and suppression of electron-hole recombination which resulted in an increase of both photocurrent and open-circuit voltage.

The application of exposed facet titania within the field of energy storage has emerged as an exciting frontier over the past several years. Energy storage technologies, such as lithium-ion batteries and supercapacitors, play a crucial role in achieving efficient energy utilization and management. Recently, many reports have also highlighted that the exposure of unusual crystal plane in TiO_2, characterized by its unique atomic arrangement and distinctive surface properties, has proven to evidently improve the efficiency, stability, and overall performance of energy storage devices. For example, a composite of hierarchically porous TiO_2 nanosheet with large exposure of (001) facet and rGO was able to exhibit a superior and stable lithium storage capacity and high performance as anode material in lithium ion batteries [141]. Based on

the result, it is reported that the anode material showed an excellent reversible capacity of 250 mAh/g in a voltage window of 1.0-3.0 V and demonstrated good stability even after 1000 cycles. In another report, Wang and co-workers compared the performance of (001)-faceted TiO_2 nanosheet vs. spherical TiO_2 nanoparticles as anode material in lithium ion batteries [142]. Here, it is evident that the battery fabricated with (001)-faceted TiO_2 nanosheet exhibited a superior storage capacity, enhanced stability, and higher charge/discharge rate that that of spherical TiO_2 nanoparticles. It is believed that such enhancement was due to the ability of exposed (001) facet in TiO_2 to facilitate an efficient charge diffusion which led to an increase in the rate of Li ion insertion/extraction along the *c*-axis during the charge-discharge.

4.2. Monolayer titanate

Most monolayer titania nanosheets are made by top-down approaches through the exfoliation of layered titanate compounds. The layered structured of titania also has many applications. Having a layered structure, the interlayer cations can be reversibly exchanged with other cations. The ion exchange properties enable the layered nanosheets to adsorb radioactive ions, hence it is useful for environmental remediation. Several researchers utilised acid modified titania nanosheets for Cs^+ ions adsorption in which the adsorption capacity did not decreased even after 5 cycles [143]. The adsorption capacity of Cs^+ ions reached 329 mg g^{-1} which is promising for radioactive wastewater treatment. Protonated TiNS were also able to adsorb cationic dyes such as methylene blue with the adsorption capacity up to 3937 mg g^{-1} following the Langmuir model [144]. For dye removal, peroxo-modification of the TiNS surface could be done, changing the colour of titania from white to yellow [135]. With hydrogen peroxide, the $Ti(IV)-H_2O_2$ complex was formed creating TiOOH moieties on the surface. The peroxo groups were then able to oxidise dyes into smaller molecules. Hence, the dye removal can be performed without the assistance of UV or visible light. The interlayer spacing and surface charge of acid modified TiNS was also induced size selectivity for adsorbing fluoroquinolone pharmaceutical [145]. In neutral and acidic solution, the acid modified TiNS were able to be intercalated by positively CIP with a thickness of 0.41 nm. Selective adsorption was also obtainable by surface modification of TiNS [128,146]. Boronic acid ligands were immobilized on the surface of modified TiNS resulting in selective adsorption of IgG up to 1669.7 mg g^{-1} capacity [146]. APTES modified TiNS was deployed as nanocontainer of DNA) [128]. The DNA was intercalated in the layer of APTES-TiNS where it was protected by TiNS from enzymatic corrosion, acid condition, and UV-vis light irradiation, thus DNA could be stored and released on demand.

The ion exchange capacity of TiNS can also facilitate energy storage. During charging and discharging, intercalation and de-intercalation of cations occur. Layered titania nanosheets with minimum layer-to-layer interaction and a robust gallery space enabled fast and stable intercalation and de-intercalation of large ions such as sodium and potassium ions in non-aqueous electrolyte [147]. To obtain minimum layer-to-layer interaction, the titania nanosheets were exfoliated via a chemical exfoliation method followed by coagulation with a Mg^{2+} solution to obtain a randomly stacked nanosheets structure. At a rate of 3000 mA g^{-1}, the capacity was retained at more than 80% after 10000 cycles for Na^+ ion storage, which was performed using electrode thickness of 80 μm. Such remarkable performances did not occur without prior exfoliation of titanates. The specific capacity for Na^+ ion storage was 53 mA h g^{-1} and 188 mA h g^{-1} respectively, without and with prior exfoliation, respectively. Nevertheless, the theoretical capacity of titanate is relatively small compared to graphite or SnO_2 [8]. Doeff *et al.* synthesised the composite of carbon-TiNS by exfoliating titanate structure followed by carbonization of dopamine for sodium half-cell configuration [148]. The hetero-structure of carbon-titania resulted in higher capacity and capacity retention while lowering the impedance.

Combination of titania nanosheets with SnO_2 for sodium ion battery should be expected in the near future. The titania nanosheets could also be used as an electrode for electroanalysis [121,130,149]. The titania nanosheet exfoliated with tetrabutylammonium cations was deposited from colloidal aqueous solution onto a glassy carbon electrode creating lamellar structure [130]. The lamellar titania acted as sorbent and host for hydrophobic redox system and for electrochemical reactivity. Future study about electron transfer, mobility, and binding of guest species within the lamellar is intriguing. The negatively charged TiNS could also act as host of ferroceneboronic acid receptor molecules exhibiting selective sensing of fructose while insensitive for glucose [149]. Moreover, cationic diode behaviour was observed using TiNS deposit on top of micron size hole of PET film [150]. The ionic current rectification was possible due to the negative surface charge of TiNS and tortuous path of ions within the lamellar space.

Titanium dioxide is known to show striking photocatalytic activities, while the high surface area of 2D nanosheets increases the density of active sites, TiNS have larger band gap (i.e., 3.84 eV) than anatase TiO_2 does (3.2 eV) [120]. Strong UV light is needed to excite the electron for photocatalysis. Therefore, many researchers combine TiNS with other catalyst to obtain narrow band gap while maintaining high surface area. One group of researchers combined positively charged Zr-EDTAcomplexes with negatively charged TiNS creating porous structure with surface area of 193 m^2 g^{-1} and specific pore volume of 0.39 mL g^{-1} [151]. The composite of Zr-EDTA-TiNS yielded a band gap of 3.15 eV and used for degrading methylene blue (MB) under UV irradiation. The photocatalytic degradation kinetic of methylene blue was 5-fold higher and reached 98.1% MB removal for Zr-EDTA-TiNS composite as compared to TiNS alone. The photocatalytic mechanism can be described as an artificial Z-scheme heterostructures due to ohmic contact facilitating charge transfer between conduction band of TiNS and valence band of Zr-EDTA. TiNS have also been combined with alkaline $Co(OH)_2$ [152] and $Ni(OH)_2$ [153] for photocatalytic reduction of CO_2. The alkaline $Co(OH)_2$ and $Ni(OH)_2$ acted as CO_2 binder while TiNS adsorbed sensitiser and became an electron relay bridging the sensitiser with $Co(OH)_2$ and $Ni(OH)_2$ active sites. For $Ni(OH)_2$-TiNS, the production rate of CO/H_2 was 1801/2093 μmol g^{-1} h^{-1} while $Co(OH)_2$-TiNS was 56.5/59.3 μmol h^{-1}. For photovoltaic application, TiNS was used as atomic stacking transporting layer (ASTL) in lead halide perovskite solar cell [154]. The TiNS were stacked into multilayer thin film by layer-by-layer deposition which achieved complete surface coverage after 5 repetitions. Contrary to the conventional sintered TiO_2 thin film, layer-by-layer deposition of TiNS exhibited nearly negligible oxygen vacancies. The oxygen vacancies may cause UV instability of perovskite solar cell. For titania nanosheets ASTL, the power conversion efficiency remained around 70% of initial value after 5 hours of UV irradiation while severe reduction of PCE occurred for the conventional TiO_2 thin film resulting in only 5% initial value of PCE. Besides photovoltaic application, TiNS could also be used for hydrovoltaic device [155]. The electricity was generated from water evaporation. The titanium vacancy of the TiNS enhanced water-solid interaction. When water molecules flow over the solid surface, the migration of counterions occurs generating electric output. The hydrovoltaic device based on TiNS produced an open circuit voltage of 1.32 V for more than 250 h.

As coating of layer-by-layer deposition of TiNS were used to protect stainless steel car baffle from corrosion [156]. The five-cycle layer-by-layer deposition of TiNS exhibited thickness around 10 nm with the corrosion inhibition efficiency of 99.92% and the estimated corrosion rate of 5.32×10^{-5} mm·year^{-1}. The 2D structure of TiNS created tortuous path for iron and oxygen diffusion hampering the rusting process of the iron. Titania nanosheets has been known as a strong adsorbent of rare earth element such as Eu exhibiting photoluminescence properties [157]. Intense red emission was observed at 616 nm under irradiation of 400 nm UV LED light.

It would be interesting to combine layers of red-emitting TiNS with blue-emitting rare-earth mixed metal oxide such as $BaMgAl_{11}O_{17}$: Eu^{2+} [158] to create multi-colour luminescent layers for monitoring coating health. As nanocomposite coating, silk-TiNS enhanced tribological properties (e.g., hardness, reduced modulus, wear, adhesion, and scratch resistance) of silk coatings [159]. The hardness and reduced modulus of silk-TiNS composite were higher than graphene-silk composite film. The reinforcement behaviour also occurred for bulk polymer nanocomposites following micromechanical models such as Halpin-Tsai and Brune-Bicerano up to few number of nanosheets layers [160]. As discussed in section 3.1.2., TiNS were sensitive to magnetic flux and UV light in which the orientation of TiNS within polymer matrix can be adjusted. Hence, stimuli-responsive polymer nanocomposites could be realised by incorporating TiNS within polymer. Silk-TiNS multilayer thin film could also exhibited moisture-responsive coating [161]. The water molecules were adsorbed into the nanosheets causing swelling and reduction of refractive index of the film. To sum up, the layered 2D structures of nanosheets, photoresponsive, chemically stable, negatively charged TiNS have many existing and potential applications worthy of further investigation in combination with other nanomaterials or polymers.

5. Conclusions and outlook

In conclusion, two-dimensional TiNS have emerged as a multifaceted and promising material that has captured the attention of the scientific community. With significant implications for fields ranging from catalysis, electronics, and energy conversion to environmental remediation, energy storage, and biomedical applications, TiNS offer a transformative potential. Key to this aspect is the manipulation of their crystal facets and structures, which allow for a tailored set of properties apt for diverse applications. Synthesis routes involving both exposed facet and monolayer titania nanosheets have demonstrated unique properties such as heightened catalytic activity, ion-exchange capabilities, and exceptional optoelectronic behaviours.

Within the realm of synthesis, hydrothermal and solvothermal methods have proven effective for facet control. There has been a shift toward non-fluorine-based precursors, primarily due to the associated safety and environmental considerations. This trend aligns well with the broader scientific movement toward more sustainable and eco-friendly materials. In contrast, the chemical exfoliation methods uses non-fluorine precursors, offering a safer yet a versatile route to monolayered structures.

For applications, TiNS demonstrate a myriad of functionalities. Their ion-exchange properties make them valuable candidates for environmental applications, such as the absorption of radioactive ions and organic dyes. The adaptability of TiNS in energy storage, particularly sodium and potassium ion batteries, and their potential in photocatalysis, signal an exciting trajectory for these materials. Composite structures have shown that TiNS can work in synergy with other materials to enhance their performance in these sectors further.

As we look to the future, the focus should be on refining and diversifying non-fluorine-based synthesis methods and deepening our understanding of the relationship between crystal structure and material properties. Exploring hybrid composites, particularly through the integration of TiNS with polymers and other nanomaterials, appears to be a promising avenue. Moreover, targeted research into nanoengineering for optimizing energy storage and tuneable band gaps for photocatalytic applications holds significant potential. These endeavours not only serve to advance our technological capabilities but also usher in an era of increased safety, energy efficiency, and environmental consciousness.

Acknowledgments

References

1   T. Edvinsson, *R. Soc. Open Sci.*, 2018, **5**, 180387.

2   D. Varsano, G. Giorgi, K. Yamashita and M. Palummo, *J. Phys. Chem. Lett.*, 2017, **8**, 3867–3873.

3   A. K. Geim and K. S. Novoselov, *Nat. Mater.*, 2007, **6**, 183–91.

4   M. Naguib, M. Kurtoglu, V. Presser, J. Lu, J. Niu, M. Heon, L. Hultman, Y. Gogotsi and M. W. Barsoum, *Adv. Mater.*, 2011, **23**, 4248–4253.

5   H. G. Yang, C. H. Sun, S. Z. Qiao, J. Zou, G. Liu, S. C. Smith, H. M. Cheng and G. Q. Lu, *Nature*, 2008, **453**, 638–641.

6   A. Fujishima and K. Honda, *Nature*, 1972, **238**, 37–38.

7   X. H. Yang, Z. Li, G. Liu, J. Xing, C. Sun, H. G. Yang and C. Li, *CrystEngComm*, 2011, **13**, 1378–1383.

8   L. Wang and T. Sasaki, *Chem. Rev.*, 2014, 114, 9455–9486.

9   M. Osada and T. Sasaki, *J. Mater. Chem.*, 2009, **19**, 2503.

10   J. S. Chen, Y. L. Tan, C. M. Li, Y. L. Cheah, D. Luan, S. Madhavi, F. Y. C. Boey, L. A. Archer and X. W. Lou, *J. Am. Chem. Soc.*, 2010, **132**, 6124–6130.

11   G. Longoni, R. L. Pena Cabrera, S. Polizzi, M. D'Arienzo, C. M. Mari, Y. Cui and R. Ruffo, *Nano Lett.*, 2017, **17**, 992–1000.

12   A. Meng, J. Zhang, D. Xu, B. Cheng and J. Yu, *Appl. Catal. B Environ.*, 2016, **198**, 286–294.

13   M. Chamtouri, B. Kenens, R. Aubert, G. Lu, T. Inose, Y. Fujita, A. Masuhara, J. Hofkens and H. Uji-I, *ACS Omega*, 2017, **2**, 4032–4038.

14   R. Ma and T. Sasaki, *Adv. Mater.*, 2010, **22**, 5082–5104.

15   B. O'Regan and M. Grätzel, *Nature*, 1991, **353**, 737–740.

16   G. Liu, H. G. Yang, J. Pan, Y. Q. Yang, G. Q. M. Lu and H. M. Cheng, *Chem. Rev.*, 2014, 114, 9559–9612.

17   T. Sasaki and M. Watanabe, *J. Am. Chem. Soc.*, 1998, **120**, 4682–4689.

18   E. L. Tae, K. E. Lee, J. S. Jeong and K. B. Yoon, *J. Am. Chem. Soc.*, 2008, **130**, 6534–6543.

19   M. Osada and T. Sasaki, *Adv. Mater.*, 2012, **24**, 210–228.

20   S. Wang, G. Liu and L. Wang, *Chem. Rev.*, 2019, **119**, 5192–5247.

21   S. Liu, J. Yu and M. Jaroniec, *Chem. Mater.*, 2011, **23**, 4085–4093.

22   Y. Wang, J. He, Y. Zhu, H. Zhang, C. Yang, K. Wang, S. Wu, Y.-L. Chueh and W. Jiang, *Appl. Surf. Sci.*, 2020, 145927.

23   W. Yao, Y. Yuan, G. Tan, C. Liu, M. Cheng, V. Yurkiv, X. Bi, F. Long, C. R. Friedrich and F. Mashayek, *J. Am. Chem. Soc.*, 2019, **141**, 12832–12838.

24   W. Q. Fang, X.-Q. Gong and H. G. Yang, *J. Phys. Chem. Lett.*, 2011, **2**, 725–734.

25   K. Lee, M. Kim and H. Kim, *J. Mater. Chem.*, 2010, **20**, 3791–3798.

26   C. Z. Wen, H. B. Jiang, S. Z. Qiao, H. G. Yang and G. Q. M. Lu, *J. Mater. Chem.*, 2011, **21**, 7052–7061.

27   Z. Jiang, Q. Kuang, Z. Xie and L. Zheng, *Adv. Funct. Mater.*, 2010, **20**, 3634–3645.

28   G. Liu, C. Y. Jimmy, G. Q. M. Lu and H.-M. Cheng, *Chem. Commun.*, 2011, **47**, 6763–6783.

29   U. Diebold, *Surf. Sci. Rep.*, 2003, **48**, 53–229.

30   A. Selloni, *Nat. Mater.*, 2008, **7**, 613–615.

31   R. Katal, S. Masudy-Panah, M. Tanhaei, M. H. D. A. Farahani and H. Jiangyong, *Chem. Eng. J.*, 2020, **384**, 123384.

32   P. Gao, D. Bao, Y. Wang, Y. Chen, L. Wang, S. Yang, G. Chen, G. Li, Y. Sun and W. Qin, *ACS Appl. Mater. Interfaces*, 2013, **5**, 368–373.

33   M. Khalil, E. S. Anggraeni, T. A. Ivandini and E. Budianto, *Appl. Surf. Sci.*, 2019, **487**, 1376–1384.

34   Y. Masuda and K. Kato, *J. Ceram. Soc. Japan*, 2009, **117**, 373–376.

35   S. E. Pratsinis and P. T. Spicer, *Chem. Eng. Sci.*, 1998, **53**, 1861–1868.

36   E. Ventosa, B. Mei, W. Xia, M. Muhler and W. Schuhmann, *ChemSusChem*, 2013, **6**, 1312–1315.

37   C. Wang, X. Zhang and Y. Liu, *Nanoscale*, 2014, **6**, 5329–5337.

38   J. R. Bourne and R. J. Davey, *J. Cryst. Growth*, 1976, **36**, 278–286.

39   C.-T. Dinh, T.-D. Nguyen, F. Kleitz and T.-O. Do, *ACS Nano*, 2009, **3**, 3737–3743.

40   M. A. Lovette, A. R. Browning, D. W. Griffin, J. P. Sizemore, R. C. Snyder and M. F. Doherty, *Ind. Eng. Chem. Res.*, 2008, **47**, 9812–9833.

41   P. M. Oliver, G. W. Watson, E. Toby Kelsey and S. C. Parker, *J. Mater. Chem.*, 1997, **7**, 563–568.

42 E. Hosono, S. Fujihara, H. Imai, I. Honma, I. Masaki and H. Zhou, *ACS Nano*, 2007, **1**, 273–278.

43 K. Kakiuchi, E. Hosono, H. Imai, T. Kimura and S. Fujihara, *J. Cryst. Growth*, 2006, **293**, 541–545.

44 T. Li, B. Tian, J. Zhang, R. Dong, T. Wang and F. Yang, *Ind. Eng. Chem. Res.*, 2013, **52**, 6704–6712.

45 C. K. Nguyen, H. G. Cha and Y. S. Kang, *Cryst. Growth Des.*, 2011, **11**, 3947–3953.

46 F. Amano, T. Yasumoto, O.-O. Prieto-Mahaney, S. Uchida, T. Shibayama and B. Ohtani, *Chem. Commun.*, 2009, 2311–2313.

47 N. Wu, J. Wang, D. N. Tafen, H. Wang, J.-G. Zheng, J. P. Lewis, X. Liu, S. S. Leonard and A. Manivannan, *J. Am. Chem. Soc.*, 2010, **132**, 6679–6685.

48 C.-W. Peng, T.-Y. Ke, L. Brohan, M. Richard-Plouet, J.-C. Huang, E. Puzenat, H.-T. Chiu and C.-Y. Lee, *Chem. Mater.*, 2008, **20**, 2426–2428.

49 C. Yang, Z. Yang, H. Gu, C. K. Chang, P. Gao and B. Xu, *Chem. Mater.*, 2008, **20**, 7514–7520.

50 L. Hou, Z. Guan, T. Liu, C. He, Q. Li and J. Yang, *Int. J. Hydrogen Energy*, 2019, **44**, 8109–8120.

51 Y. Jun, J.-H. Lee, J. Choi and J. Cheon, *J. Phys. Chem. B*, 2005, **109**, 14795–14806.

52 Y. Yin and A. P. Alivisatos, *Nature*, 2005, **437**, 664–670.

53 P. P. Ahonen, A. Moisala, U. Tapper, D. P. Brown, J. K. Jokiniemi and E. I. Kauppinen, *J. Nanoparticle Res.*, 2002, **4**, 43–52.

54 F. Amano, O.-O. Prieto-Mahaney, Y. Terada, T. Yasumoto, T. Shibayama and B. Ohtani, *Chem. Mater.*, 2009, **21**, 2601–2603.

55 Y. Alivov and Z. Y. Fan, *J. Phys. Chem. C*, 2009, **113**, 12954–12957.

56 Y. Alivov and Z. Y. Fan, *Nanotechnology*, 2009, **20**, 405610.

57 L. Chu, Z. Qin, J. Yang and X. Li, *Sci. Rep.*, 2015, **5**, 12143.

58 S. M. Lee, G. C. Park, T. Y. Seo, S.-B. Jung, J. H. Lee, Y. D. Kim, D. H. Choi, J. H. Lim and J. Joo, *Nanotechnology*, 2016, **27**, 395604.

59 B. Wang, L. Guo, M. He and T. He, *Phys. Chem. Chem. Phys.*, 2013, **15**, 9891–9898.

60 S. Weon, E. Choi, H. Kim, J. Y. Kim, H.-J. Park, S. Kim, W. Kim and W. Choi, *Environ. Sci. Technol.*, 2018, **52**, 9330–9340.

61 L. Chen, L. Shen, P. Nie, X. Zhang and H. Li, *Electrochim. Acta*, 2012, **62**, 408–415.

62 J. Zhu, S. Wang, Z. Bian, S. Xie, C. Cai, J. Wang, H. Yang and H. Li, *CrystEngComm*, 2010, **12**, 2219–2224.

63 N. Liu, Y. Chang, Y. Feng, Y. Cheng, X. Sun, H. Jian, Y. Feng, X. Li and H. Zhang,

ACS Appl. Mater. Interfaces, 2017, **9**, 5907–5915.

64   X. Han, X. Wang, S. Xie, Q. Kuang, J. Ouyang, Z. Xie and L. Zheng, *Rsc Adv.*, 2012, **2**, 3251–3253.

65   G. Liu, J. Pan, L. Yin, J. T. S. Irvine, F. Li, J. Tan, P. Wormald and H. Cheng, *Adv. Funct. Mater.*, 2012, **22**, 3233–3238.

66   Z. Zhao, Z. Sun, H. Zhao, M. Zheng, P. Du, J. Zhao and H. Fan, *J. Mater. Chem.*, 2012, **22**, 21965–21971.

67   M. Khalil, T. H. Rangkuti, F. Naumi, J. Gunlazuardi, T. A. Ivandini, G. T. M. Kadja and J. Y. Mulyana, *Inorg. Chem. Commun.*, 2020, **118**, 107992.

68   J. S. Chen, J. Liu, S. Z. Qiao, R. Xu and X. W. D. Lou, *Chem. Commun.*, 2011, **47**, 10443–10445.

69   I. E. Grey, C. Li, I. C. Madsen and J. a. Watts, *J. Solid State Chem.*, 1987, **66**, 7–19.

70   A. R. West, *Solid State Chemistry and Its Applications*, John Wiley & Sons, 1987.

71   T. Kimura, in *Advances in Ceramics - Synthesis and Characterization, Processing and Specific Applications*, IntechOpen, 2011.

72   M. R. Allen, A. Thibert, E. M. Sabio, N. D. Browning, D. S. Larsen and F. E. Osterloh, *Chem. Mater.*, 2010, **22**, 1220–1228.

73   T. Sasaki, M. Watanabe, Y. Michiue, Y. Komatsu, F. Izumi and S. Takenouchi, *Chem. Mater.*, 1995, **7**, 1001–1007.

74   M. Iida, T. Sasaki and M. Watanabe, *Chem. Mater.*, 1998, **10**, 3780–3782.

75   T. Tanaka, Y. Ebina, K. Takada, K. Kurashima and T. Sasaki, *Chem. Mater.*, 2003, **15**, 3564–3568.

76   J.-H. Choy and Y.-S. Han, *Mater. Lett.*, 1998, **34**, 111–118.

77   M. Yokoyama, T. Ota and I. Yamai, *J. Mater. Sci.*, 1989, **24**, 3787–3790.

78   R. Ma, Z. Liu, L. Li, N. Iyi and T. Sasaki, *J. Mater. Chem.*, 2006, **16**, 3809.

79   Y. Omomo, T. Sasaki, L. Wang and M. Watanabe, *J. Am. Chem. Soc.*, 2003, **125**, 3568–3575.

80   C. Harito, D. V. Bavykin and F. C. Walsh, in *IOP Conference Series: Materials Science and Engineering*, 2017, vol. 223, p. 012054.

81   G. Hu, L. Yi and C. Liu, *J. Supercrit. Fluids*, 2012, **72**, 59–67.

82   N. Sukpirom and M. M. Lerner, *Mater. Sci. Eng. A*, 2002, **333**, 218–222.

83   T. Orzali, M. Casarin, G. Granozzi, M. Sambi and A. Vittadini, *Phys. Rev. Lett.*, 2006, **97**, 1–4.

84   G. Kim, C. Jo, W. Kim, J. Chun, S. Yoon, J. Lee and W. Choi, *Energy Environ. Sci.*, 2013, **6**, 2932–2938.

85   A. Funatsu, M. Koinuma, T. Taniguchi, K. Hatakeyama, Y. Okazawa, Y. Fukunaga, H. Tateishi, C. Ogata and Y. Matsumoto, *RSC Adv.*, 2013, **3**, 21343.

86   K. Nakamura, Y. Oaki and H. Imai, *J. Am. Chem. Soc.*, 2013, **135**, 4501–4508.

87   T. Ban, T. Nakagawa and Y. Ohya, *Cryst. Growth Des.*, 2015, **15**, 1801–1807.

88   T. Gao, H. Fjellvåg and P. Norby, *J. Mater. Chem.*, 2009, **19**, 787–794.

89   N. Miyamoto, K. Kuroda and M. Ogawa, *J. Mater. Chem.*, 2004, **14**, 165–170.

90   L. Liu, Z. Liu, A. Liu, X. Gu, C. Ge, F. Gao and L. Dong, *ChemSusChem*, 2014, **7**, 618–626.

91   L. Ye, J. Mao, J. Liu, Z. Jiang, T. Peng and L. Zan, *J. Mater. Chem. A*, 2013, **1**, 10532–10537.

92   L. Liu, Y. Jiang, H. Zhao, J. Chen, J. Cheng, K. Yang and Y. Li, *Acs Catal.*, 2016, **6**, 1097–1108.

93   S. Illa, R. Boppella, S. V Manorama and P. Basak, *J. Phys. Chem. C*, 2016, **120**, 18028–18038.

94   Q. Wu, M. Liu, Z. Wu, Y. Li and L. Piao, *J. Phys. Chem. C*, 2012, **116**, 26800–26804.

95   W. Chen, Q. Kuang, Q. Wang and Z. Xie, *Rsc Adv.*, 2015, **5**, 20396–20409.

96   X.-Q. Gong, A. Selloni and A. Vittadini, *J. Phys. Chem. B*, 2006, **110**, 2804–2811.

97   G. Liu, C. Sun, H. G. Yang, S. C. Smith, L. Wang, G. Q. M. Lu and H.-M. Cheng, *Chem. Commun.*, 2010, **46**, 755–757.

98   J. Pan, G. Liu, G. Q. Lu and H. Cheng, *Angew. Chemie Int. Ed.*, 2011, **50**, 2133–2137.

99   J. Pan, X. Wu, L. Wang, G. Liu, G. Q. M. Lu and H.-M. Cheng, *Chem. Commun.*, 2011, **47**, 8361–8363.

100   H. Xu, P. Reunchan, S. Ouyang, H. Tong, N. Umezawa, T. Kako and J. Ye, *Chem. Mater.*, 2013, **25**, 405–411.

101   M. Dahl, Y. Liu and Y. Yin, *Chem. Rev.*, 2014, **114**, 9853–9889.

102   J. Schneider and D. W. Bahnemann, *J. Phys. Chem. Lett.*, 2013, **4**, 3479–3483.

103   J.-D. Peng, P.-C. Shih, H.-H. Lin, C.-M. Tseng, R. Vittal, V. Suryanarayanan and K.-C. Ho, *Nano Energy*, 2014, **10**, 212–221.

104   W. Sun, T. Peng, Y. Liu, W. Yu, K. Zhang, H. F. Mehnane, C. Bu, S. Guo and X.-Z. Zhao, *ACS Appl. Mater. Interfaces*, 2014, **6**, 9144–9149.

105   X. Wu, Z. Chen, G. Q. Lu and L. Wang, *Adv. Funct. Mater.*, 2011, **21**, 4167–4172.

106   Y. Zhang, J. Cai, Y. Ma and L. Qi, *Nano Res.*, 2017, **10**, 2610–2625.

107   J. Yu, J. Low, W. Xiao, P. Zhou and M. Jaroniec, *J. Am. Chem. Soc.*, 2014, **136**, 8839–8842.

108   X.-Q. Gong and A. Selloni, *J. Phys. Chem. B*, 2005, **109**, 19560–19562.

109   M. Lazzeri, A. Vittadini and A. Selloni, *Phys. Rev. B*, 2001, **63**, 155409.

110   A. Vittadini, A. Selloni, F. P. Rotzinger and M. Grätzel, *Phys. Rev. Lett.*, 1998, **81**, 2954.

111   L. Liu, X. Gu, Z. Ji, W. Zou, C. Tang, F. Gao and L. Dong, *J. Phys. Chem. C*, 2013, **117**, 18578–18587.

112   Z. He, L. Jiang, D. Wang, J. Qiu, J. Chen and S. Song, *Ind. Eng. Chem. Res.*, 2015, **54**, 808–818.

113   L. Yan, J. Du and C. Jing, *Catal. Sci. Technol.*, 2016, **6**, 2419–2426.

114   R. Ma, Y. Bando and T. Sasaki, *Chem. Phys. Lett.*, 2003, **380**, 577–582.

115   R. Ma, K. Fukuda, T. Sasaki, M. Osada and Y. Bando, *J. Phys. Chem. B*, 2005, **109**, 6210–6214.

116   T. Sasaki, Y. Ebina, T. Tanaka, M. Harada, L. Pasteur and I. C. Sadron, *Chem.Mater.*, 2001, **13**, 4661–4667.

117   H. J. Kim, M. Osada, Y. Ebina, W. Sugimoto, K. Tsukagoshi and T. Sasaki, *Sci. Reports 2016 61*, 2016, **6**, 1–9.

118   X. Wang, X. Li, S. Aya, F. Araoka, Y. Ishida, A. Kikkawa, M. Kriener, Y. Taguchi, Y. Ebina, T. Sasaki, S. Koshiya, K. Kimoto and T. Aida, *J. Am. Chem. Soc.*, 2018, **140**, 16396–16401.

119   N. Sakai, Y. Ebina, K. Takada and T. Sasaki, *J. Am. Chem. Soc.*, 2004, **126**, 5851–5858.

120   T. Sasaki and M. Watanabe, *J. Phys. Chem. B*, 1997, **101**, 10159–10161.

121   B. Fan, Y. Zhao, B. R. Putra, C. Harito, D. Bavykin, F. C. Walsh, M. Carta, R. Malpass-Evans, N. B. McKeown and F. Marken, *Electroanalysis*, 2020, **32**, 2756–2763.

122   A. Tanaka, K. Hatakeyama, A. Oku, K. Matsuzaki, N. Saitou, H. Yokoi, T. Taniguchi, Y. Matsumoto and M. Hara, *Appl. Phys. Lett.*, 2014, **104**, 163106.

123   S. Liu, J. Yu and M. Jaroniec, *J. Am. Chem. Soc.*, 2010, **132**, 11914–11916.

124   F. Amano, T. Yasumoto, O. O. P. Mahaney, S. Uchida, T. Shibayama, Y. Terada and B. Ohtani, *Top. Catal.*, 2010, **53**, 455–461.

125   B. Wu, C. Guo, N. Zheng, Z. Xie and G. D. Stucky, *J. Am. Chem. Soc.*, 2008, **130**, 17563–17567.

126   T. Tachikawa, S. Yamashita and T. Majima, *J. Am. Chem. Soc.*, 2011, **133**, 7197–7204.

127   N. Murakami, Y. Kurihara, T. Tsubota and T. Ohno, *J. Phys. Chem. C*, 2009, **113**, 3062–3069.

128   T. W. Kim, I. Y. Kim, D.-H. Park, J.-H. Choy and S.-J. Hwang, *Sci. Rep.*, 2016, **6**, 21993.

129   M. Osada and T. Sasaki, *Polym. J.*, 2015, **47**, 89–98.

130   W. T. Wahyuni, B. R. Putra, C. Harito, D. V Bavykin, F. C. Walsh, P. J. Fletcher and F. Marken, *Anal. Chim. Acta X*, 2019, **1**, 100001.

131   S. Z. J. Zaidi, C. Harito, F. C. Walsh and C. Ponce de León, *J. Solid State Electrochem.*, 2018, **22**, 2889–2900.

132   A. S. Martins, C. Harito, D. V. Bavykin, F. C. Walsh and M. R. V. Lanza, *J. Mater. Chem. C*, 2017, **5**, 3955–3961.

133   D. V. Bavykin and F. C. Walsh, *Titanate and Titania Nanotubes*, Royal Society of Chemistry, Cambridge, 2009.

134   D. V. Bavykin, J. M. Friedrich and F. C. Walsh, *Adv. Mater.*, 2006, **18**, 2807–2824.

135   C. Zhou, J. Luo, Q. Chen, Y. Jiang, X. Dong and F. Cui, *Chem. Commun.*, 2015, **51**, 10847–10849.

136   T. Wu, X. Kang, M. W. Kadi, I. Ismail, G. Liu and H.-M. Cheng, *Chinese J. Catal.*, 2015, **36**, 2103–2108.

137   R. T. Yunarti, T. N. Safitri, L. C. C. Dimonti, G. Aulia, M. Khalil and M. Ridwan, *J. Phys. Chem. Solids*, 2022, **160**, 110357.

138   M. Khalil, F. Naumi, U. Pratomo, T. A. Ivandini, G. T. M. Kadja and J. Y. Mulyana, *Appl. Surf. Sci.*, 2021, **542**, 148746.

139   S. M. H. Qaid, H. M. Ghaithan, H. S. Bawazir, A. F. Bin Ajaj, K. K. AlHarbi and A. S. Aldwayyan, *Nanomaterials*, 2023, 13.

140   M. M. Maitani, A. Tateyama, P. P. Boix, G. Han, A. Nitta, B. Ohtani, N. Mathews and Y. Wada, *Electrochim. Acta*, 2019, **300**, 445–454.

141   W.-B. Yu, Z.-Y. Hu, J. Jin, M. Yi, M. Yan, Y. Li, H.-E. Wang, H.-X. Gao, L.-Q. Mai, T. Hasan, B.-X. Xu, D.-L. Peng, G. Van Tendeloo and B.-L. Su, *Natl. Sci. Rev.*, 2020, **7**, 1046–1058.

142   Z. Wang, Y. Zhang, T. Xia, J. Murowchick, G. Liu and X. Chen, *Energy Technol.*, 2014, **2**, 376–382.

143   W. Geng, D. Wang, Y. Liu, J. Zhang, L. Zhong, R. Lin, L. Ding, L. Wu and D. Dong, *Hydrometallurgy*, 2023, **216**, 105999.

144   H. Yuan, S. Ma, X. Wang, H. Long, X. Zhao, D. Yang, W. H. Lo and Y. H. Tsang, *RSC Adv.*, 2019, **9**, 5891–5894.

145   Q. Wu, X. Yang, J. Liu, X. Nie, Y. Huang, Y. Wen, J. Khan, W. U. Khan, M. Wu and T. An, *ACS Appl. Mater. Interfaces*, 2014, **6**, 17730–17739.

146   P. F. Guo, X. M. Wang, M. M. Wang, T. Yang, M. L. Chen and J. H. Wang, *Nanoscale*, 2019, **11**, 9362–9368.

147 J. Yang, X. Xiao, W. Gong, L. Zhao, G. Li, K. Jiang, R. Ma, M. H. Rummeli, F. Li, T. Sasaki and F. Geng, *Angew. Chemie - Int. Ed.*, 2019, **58**, 8740–8745.

148 G. Barim, R. Dhall, E. Arca, T. R. Kuykendall, W. Yin, K. J. Takeuchi, E. S. Takeuchi, A. C. Marschilok and M. M. Doeff, *ACS Appl. Nano Mater.*, 2022, **5**, 678–690.

149 W. Tri Wahyuni, B. Riza Putra, C. Harito, D. V. Bavykin, F. C. Walsh, T. D. James, G. Kociok-Köhn and F. Marken, *Electroanalysis*, 2018, **30**, 1303–1310.

150 B. R. Putra, C. Harito, D. V. Bavykin, F. C. Walsh, W. T. Wahyuni, J. A. Boswell, A. M. Squires, J. M. F. Schmitt, M. A. Da Silva, K. J. Edler, P. J. Fletcher, A. E. Gesell and F. Marken, *J. Solid State Electrochem.*, 2019, **23**, 1237–1248.

151 D. Sun, Z. Lin, S. Xiao, Q. Yin and L. He, *J. Porous Mater.*, 2019, **26**, 1639–1648.

152 W. Liao, W. Chen, S. Lu, S. Zhu, Y. Xia, L. Qi, M. Q. Yang and S. Liang, *ACS Appl. Mater. Interfaces*, 2021, **13**, 38239–38247.

153 W. Liao, S. Lu, W. Chen, S. Zhu, Y. Xia, M. Q. Yang and S. Liang, *Green Chem. Eng.*, 2022, **3**, 240–249.

154 T. P. Chen, C. W. Lin, S. S. Li, Y. H. Tsai, C. Y. Wen, W. J. Lin, F. M. Hsiao, Y. P. Chiu, K. Tsukagoshi, M. Osada, T. Sasaki and C. W. Chen, *Adv. Energy Mater.*, 2018, **8**, 1701722.

155 C. Liu, C. Ye, Y. Wu, Y. Liu, Z. Liu, Z. Chen, R. Ma, N. Sakai, L. Xue, J. Sun, W. Zhang, W. Zhang, X. Wang, T. Sasaki, P. Xiong and J. Zhu, *Nano Energy*, 2023, **110**, 108348.

156 L. Nurdiwijayanto, H. Nishijima, Y. Miyake, N. Sakai, M. Osada, T. Sasaki and T. Taniguchi, *Nano Lett.*, 2021, **21**, 7044–7049.

157 E. Colusso, D. Vitiello, G. Perotto, G. Valotto, E. Cattaruzza and A. Martucci, *Adv. Mater. Interfaces*, 2019, **6**, 1800992.

158 Y. He, S. C. Wang, F. C. Walsh, W. S. Li, L. He and P. A. S. Reed, *RSC Adv.*, 2015, **5**, 42965–42970.

159 J. A. Arsecularatne, E. Colusso, E. Della Gaspera, A. Martucci and M. J. Hoffman, *Tribol. Int.*, 2020, **146**, 106195.

160 C. Harito, D. V. Bavykin, M. E. Light and F. C. Walsh, *Compos. Part B Eng.*, 2017, **124**, 54–63.

161 E. Colusso, G. Perotto, Y. Wang, M. Sturaro, F. Omenetto and A. Martucci, *J. Mater. Chem. C*, 2017, **5**, 3924–3931.